Andreas Krenn, BSc

Energy-Limited Hydrodynamic Escape: An Investigation Of The Range of Applicability

MASTER'S THESIS

to achieve the university degree of

Master of Science

Master's degree programme: Physics

submitted to

Graz University of Technology

Supervisor

Helmut Lammer, Priv.-Doz. Mag. Dr.

Institute of Physics, University of Graz

in cooperation with the Space Research Institute of the Austrian Academy of Sciences

Graz, September 2020

AFFIDAVIT

I declare that I have authored this thesis independently, that I have not used other than the declared sources/resources, and that I have explicitly indicated all material which has been quoted either literally or by content from the sources used. The text document uploaded to TUGRAZonline is identical to the present master's thesis.

Date, Signature

Nobody ever figures out what life is all about. And it doesn't matter. Explore the world. Nearly everything is really interesting if you go into it deeply enough.

Richard P. Feynman

Abstract

Energy-limited hydrodynamic escape: an investigation of the range of applicability

A protoplanet can catch a significant envelope of hydrogen gas while forming within the protoplanetary disc. Once the disc has disappeared, this envelope will start to interact with the incident extreme ultraviolet and X-ray (XUV) radiation of the host star. The XUV radiation is absorbed in the upper atmosphere. If the incident XUV energy is high enough this can drive hydrodynamic escape, leading to the loss of particles. An upper limit to the maximum particle escape driven by XUV radiation can be found, when looking at the amount of available XUV energy. Watson et al. [1981] did such an investigation of the energy-limited escape rate for the first time. They provided a set of equations to calculate the height of the XUV absorption in the atmosphere and the maximum particle escape rate. However, they used a variety of assumptions that limit the scope of applicability of the equations, like a thin XUV absorption layer in the upper atmosphere and an absorption of all the XUV energy below the sonic level of the system. This thesis provides an thorough investigation of these assumptions and compares the solution of the energy-limited equations with results from hydrodynamic simulations. It argues why the energy-limited escape formalism is not a reliable estimator of atmospheric mass-loss rates when studying planetary evolution. Finally, it offers explanations for the failure of the energy-limited approach, which potentially may be used to improve the approximation to estimate atmospheric escape rates better.

Contents

Acknowledgements

I want to thank Priv.-Doz. Mag. Dr. Helmut Lammer for his outstanding supervision of this thesis as well as the opportunity to work with him and his team on this project. I also want to thank him and the Austrian Academy of Sciences for the sponsorship of the attendance of the 10th Moscow Solar System Symposium at the Russian Space Research Institute IKI and the young scientists meeting at the Institute of Astronomy of the Russian Academy of Sciences in 2019.

I also greatly appreciate the advice and support provided by Priv.-Doz. Dr. Luca Fossati and Darya Kubyshkina, Ph.D. I also want to thank them for the opportunity to use the data they have produced with their hydrodynamic simulations.

Finally, I want to thank my family and friends, especially my parents Andrea and Andreas Krenn as well as Frederik Wilfan and Magdalena Lienhart, who have supported me throughout my studies and have always shown a lot of understanding for the time I invested in it.

1 Introduction

Back in 1981 planetary science and the study of atmospheric evolution was limited to a very small sample size. Only 8 (counting in Pluto 9) planets were known and only from three of them, Venus, Earth and Mars, significant atmospheric data had been acquired by space missions. It therefore seems obvious that the description of the evolution of a planetary atmosphere was a difficult task, since any predictions a theoretical model would produce were hard to compare with real experimental evidence. Nevertheless, the question of the origin and evolution of the solar system was still a burning one and one many scientists from a variety of different scientific fields (astrophysics, geophysics, geology,...) tried to answer.

To do so a number of theoretical models that tried to simulate the formation and subsequent evolution of the solar system like Dermott [1978] and Atreya et al. [1989] were published. However, researchers soon realized that when starting with any reasonable initial conditions within the stellar nebula, it was basically impossible to arrive at the today known properties of the planetary bodies, without adding a variety of additional processes that would further drive the evolution after their formation.

One of this formation theories is the so called "fast growth model", which will be discussed in section 2.1. This theory, which is still highly favoured by many scientists today, is able to explain the masses and positions of the planets in the solar system very well. However, because of the fast accretion of mass within the solar nebula, this formation theory also allows for the planets to acquire an extensive hydrogen envelope (see Figure 1). This hydrogen envelope can not be observed today at any terrestrial planet. In addition recent research such as Cubillos et al. [2017] indicates the importance of hydrogen escape in the evolution of planetary atmospheres by explaining abundances of observed planetary systems. Mechanisms that remove hydrogen envelopes over the course of the evolution of a planet must therefore be investigated [Lammer, 2013; Erkaev et al., 2013].

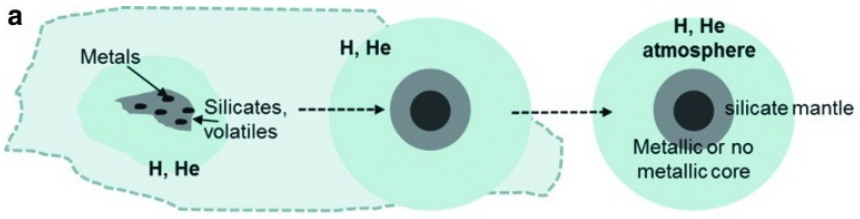

Figure 1: Illustration of the formation and accretion of dense hydrogen-gas envelopes around the rocky cores of young terrestrial planets within the protoplanetary nebula [Erkaev et al., 2013].

The removal of this envelope is usually attributed to hydrodynamic escape driven by solar extreme ultraviolet and X-ray (XUV) radiation. In the above mentioned year 1981, when planetary science was still in its early phases, Andrew J. Watson, Thomas M. Donahue and James C. G. Walker came up with a theoretical concept to estimate the maximum particle loss rate this interaction of solar XUV radiation and the planetary hydrogen atmospheres could produce [Watson et al., 1981].

They therefore allowed to quantify how fast an acquired hydrogen envelope could be removed by hydrodynamic escape over the course of the evolution of a planet. This theoretical model was called energy-limited escape and ought to provide an upper limit for the particle loss rate.

However, because of the lack of different systems to apply their formalism to, their work initially was confined to the planets of the solar system, where the formalism was used to estimate the atmospheric escape rates from Venus, Earth and Mars. With the discovery of the first exoplanets by Mayor and Queloz [1995] and space telescopes like CoRoT (e.g. Moutou et al. [2013]) and Kepler (e.g. Borucki et al. [2010]) as well as ground-based observations (for example microlensing detection e.g. Gaudi [2012]) it has found a much broader field of application. Figure 2 shows the relation of radius to orbital period for all exoplanets confirmed before December 2017. As can be seen a variety of peculiar systems unlike any in our solar system were observed.

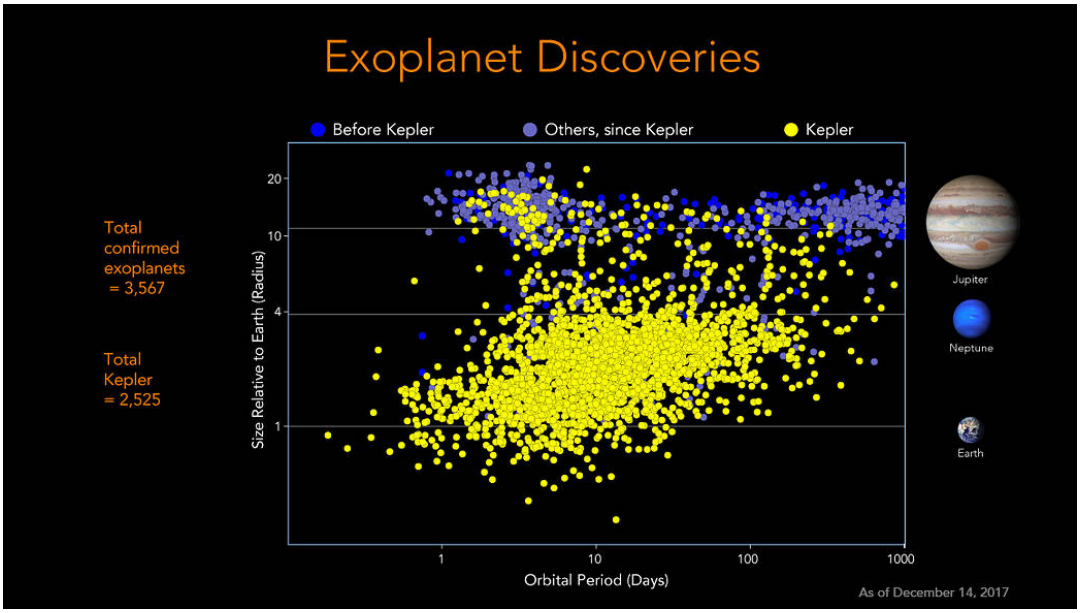

Figure 2: Overview of radius to orbital period relation of all exoplanets confirmed before December 2017 [NASA, 2017].

Simultaneous developments in the field of solar physics implied by observations of near Sun-like stars that the early Sun had much higher XUV fluxes than previously considered. This let to the energy-limited escape formalism being used by many researchers to estimate the impact of XUV radiation on atmospheric evolution at different planetary systems. Valencia et al. [2010], Owen and Wu [2013] and Luger and Barnes [2015] are all examples for recent research using an energy-limited approach to approximate hydrodynamic escape.

However, the theoretical model proposed by Watson et al. [1981] includes a variety of assumptions and limitations that limit the use of the the energy-limited formalism. It is highly questionable, whether the model can describe exotic systems, with parameters like high temperatures, high stellar energy inputs or low gravitational potential. The aim of this investigation is to examine these assumptions and limitations in detail and to provide boundaries for the applicability of the formalism.

To do so a detailed examination of the original paper Watson et al. [1981] including a thorough investigation of all the assumptions and limitations used in the derivation of the theoretical model is provided in the beginning. Chapter 6 compares different methods of obtained energy-limited mass-loss rates and analyzes their dependence on the planetary parameters. The results of the energy-limited escape formalism are compared with results acquired in hydrodynamic simulations performed by Kubyshkina et al. [2018a] in chapter 7. Finally a conclusion on the applicability of the energy-limited escape formalism is drawn in chapter 8.

2 The Introduction of the energy-limited escape theory in 1981

In 1981 Andrew J. Watson, Thomas M. Donahue and James C. G. Walker published their paper "The Dynamics of a Rapidly Escaping Atmosphere: Applications to the Evolution of Earth and Venus" [Watson et al., 1981], in which they introduced the idea of energy-limited escape for the first time. This chapter will investigate the different parts of this paper in detail, explain the energy-limited escape formalism and highlight assumptions used in the publication.

2.1 Fast accretion and hydrogen envelopes

Watson et al. [1981] start by specifying the type of system they want to consider. Their description reads:

> "We consider the case of a planetary atmosphere after the solar nebula has dissipated. We assume an extensive thermosphere of molecular or atomic hydrogen that contains a negligible amount of dust." [Watson et al., 1981]

The authors clearly assume already in the beginning of their investigation the presence of a hydrogen envelope around a massive planetary body. To understand hydrodynamic escape of hydrogen envelopes one must therefore first answer, how planetary evolution looks in a system that forms such a massive hydrogen envelope. Planetary systems form after the collapse of a molecular cloud gives rise to the birth of a new star. The gas and dust in this cloud starts rotating around the host star as it spirals inward, forming a disc like structure. In this disc planetary embryos can be formed by gravitational instabilities and collisions [Jacobsen and Harper, 1996; Jacobsen et al., 2008; Lammer et al., 2014; Stökl et al., 2016]. At the beginning of the systems evolution this embryos are still embedded in a gas cloud that is pulled in towards the host star. This gas cloud is usually referred to as *protosolar nebula* and has the same abundances (mainly hydrogen and helium) as the host star itself. It takes about 10 Myrs for this nebula to dissipate [Montmerle et al., 2006; Jacobsen et al., 2008; Lammer et al., 2018]. In the case of the solar system, Bollard et al. [2017] and Wang et al. [2017] estimate the nebula lifetime at around 3 to 5 Myrs.

Figure 3 shows the extend of the accreted hydrogen envelope for different core masses and different nebula lifetimes. As can be seen here, planetary embryos with a mass of only a few tenth of an Earth mass are able to capture a significant hydrogen envelope within the nebula lifetime. If they are massive enough by the time the disc dissipates, they are able to keep a significant envelope even after the thermal loss of

the majority of the initially captured hydrogen. This means that in order to have an extensive hydrogen thermosphere, the planet needs to accumulate a mass of few tenth of an Earth mass within the first 10 Myrs of the evolution of the stellar system [Stökl et al., 2016].

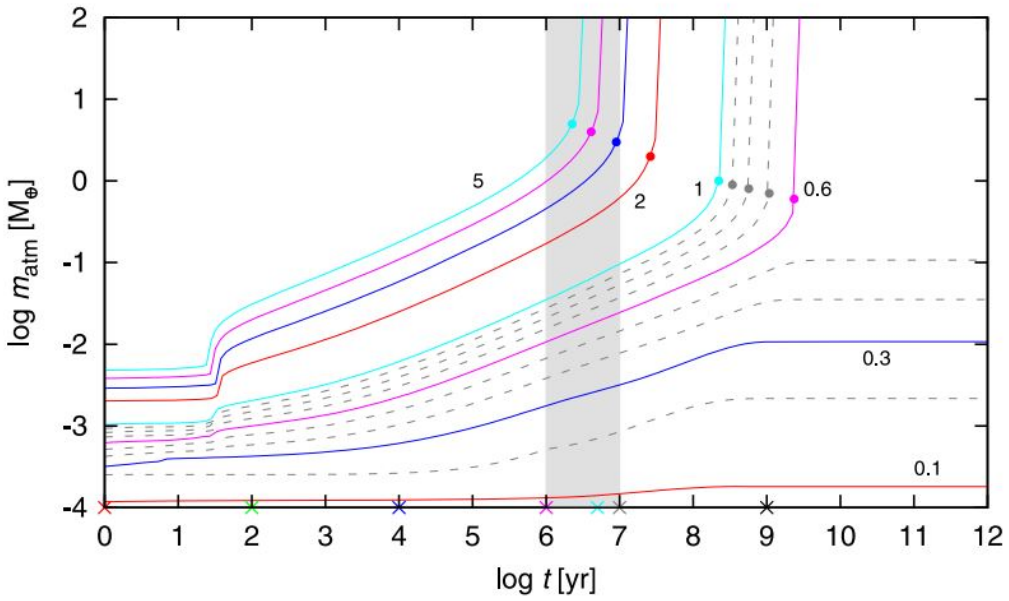

Figure 3: Total mass of accumulated hydrogen envelopes as a function of time. The lines correspond to protoplanetary core masses of 0.1, 0.2, 0.3, 0.4, 0.5, 0.6, 0.7, 0.8, 0.9. 1.0, 2.0, 3.0, 4.0 and 5.0 Earth masses. The shaded area highlights the typical lifetime of the protosolar nebula [Stökl et al., 2016].

Back in 1981, when Watson et al. published their original paper, the classical core-accretion model (Bodenheimer and Pollack [1986]; Pollack et al. [1996]) was not even introduced yet. However, first ideas that later led to this theory, were published in 1969 by Safronov and Zvjagina [1969] and in 1980 by Wetherill [1980]. This classical core-accretion model expects planetary formation to take place over 100 - 200 Myrs, starting very slowly with dust accumulation due to gravitational instabilities and only picking up pace in the final stage of planetary formation when the gravitational potential of the protoplanets becomes high.

However, the classical core-accretion model has significant problems explaining the evolution of Mars as its mass is much lower than it should be according to classical core-accretion model simulations. Much more recently suggested formation models of the Solar System such as Walsh et al. [2011], the Grand Tack model of O'Brien et al.

[2014] and the pebble accretion model by Izidoro et al. [2019] allow for much faster planetary formation. They use a combination of planetesimal collision, accretion of centimeter to meter sized particles (so called pebbles) aided by aerodynamic drag in the gas disc and planetary migration. Using these models, proto-Earth can have grown up to 0.75 Earth masses and proto-Venus even up to 1 Venus mass within the first 10 Myrs [Lammer et al., 2020].

To summarize, the formation of planetary systems is still a highly debated problem. But recent studies support fast growth models as opposed to the classical slow growth core-accretion model. A fast growth model would allow a protoplanet to accumulate an extensive hydrogen envelope setting the basis for the further investigation of possible hydrodynamic escape of this envelope and therefore justifies the starting point of the investigation of Watson et al. [1981].

2.2 Escape processes

After establishing the possibility of an extended hydrogen envelope around a young planetary body, the question arises how this hydrogen can be removed from the system again. The main requirement is for a particle to gain enough energy to reach a velocity that is higher than the local escape velocity v_{esc} (the velocity needed to overcome the gravitational potential of the planet). Two major categories must be distinguished in the description of such atmospheric escape processes: Thermal and non-thermal escape [Chamberlain, 1963; Catling and Zahnle, 2009; Coates, 2010; Lammer, 2013].

2.2.1 Thermal escape processes

The particles within a gas in thermodynamic equilibrium do not all have the same thermal energy and therefore the same velocity. Due to collisions within the gas and the surrounding medium the individual particles have velocities that are randomly selected from a so called Maxwell-Boltzmann distribution. The most probable velocity of a particle v_0 in a gas with this distribution is given as [Chamberlain, 1963]:

$$v_0 = \sqrt{\frac{2kT}{m}} \tag{1}$$

where k is the Boltzmann constant, T the temperature of the gas and m the weight of the particle. In Figure 4 a typical velocity distribution of hydrogen and oxygen molecules in Earth's exosphere with a temperature of 1000 K is shown. The exosphere is the outermost region of a planetary atmosphere. It is so thin that particles can travel essentially collision less on ballistic trajectories. As can be seen here a significant fraction of hydrogen molecules can have velocities higher than the escape

velocity even though the most probable velocity is far below it. When the velocity vector of these particles is directed away from the planet and no further collision stops them, the particles can escape the gravitational potential of the planet and leave the system [Bauer and Lammer, 2004; Coates, 2010].

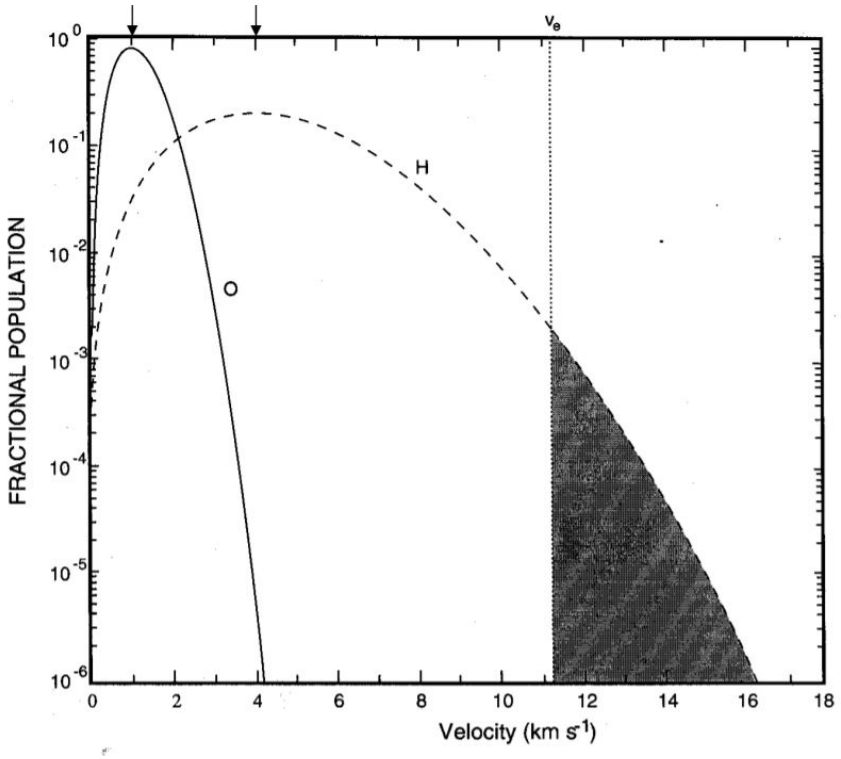

Figure 4: Boltzmann distribution for hydrogen and oxygen molecules in Earths exosphere with a temperature of 1000 K. The dark shaded area marks the part of the distribution where the hydrogen atoms have reached velocities above the escape velocity of Earth [Coates, 2010].

Jeans escape

This exact case was first treated by Sir James Jeans. He assumed a gas in thermodynamic equilibrium in which the velocities of the particles are distributed according to a Maxwellian velocity distribution. The gas is situated in the exosphere. He then proceeded to calculate how many particles in this system would be able to escape accounting for particle velocities from the distribution and the direction of the velocity vectors. This calculation resulted in the Jeans formula for escape by thermal evaporation [Chamberlain, 1963]:

$$\Phi_{escape} = \frac{n(z)v_0}{2\sqrt{\pi}} \left(\frac{v_{esc}^2}{v_0^2} + 1 \right) e^{-\frac{v_{esc}^2}{v_0^2}} \tag{2}$$

where Φ_{escape} represents the particle escape flux and $n(z)$ the number density as a function of atmospheric height z. This so called Jeans escape is an important loss process in many planetary systems and can be easily calculated with the above mentioned formula. It is also the only escape process working on every body with an gaseous envelope [Chamberlain, 1963; Bauer and Lammer, 2004].

Hydrodynamic escape

Below the above mentioned exosphere, where particles can essentially travel collision less, lies the collision dominated regime of the atmosphere. Here the gas behaves mostly like a fluid and can be described by hydrodynamic equations. The gas is heated at the planetary surface as a result of the equilibrium condition of incident stellar radiation and planetary infrared (or heat) radiation. From the surface on the gas expands radially upwards. This expansion leads to a cooling of the gas and a drop in particle density and pressure with increasing height. This results in an upward flow motion of the gas, which is counteracted by the gravitational attraction of the planet. As the particles flow upward their thermal energy is converted to kinetic energy, while the force of gravity counteracts the resulting acceleration. If the thermal energy of the gas is high enough, the upward flow of particles can overcome the gravitational potential of the planet and the particles can reach escape velocity at a certain height in the atmosphere. The particles then flow off the planet in a bulk an no longer merely evaporate. This way a large amount of gas can escape and lighter molecules can even drag heavier molecules along with them trough collisions [Catling and Zahnle, 2009; Lammer, 2013].

There are two possible ways for the atmosphere to acquire thermal energies high enough to cause hydrodynamic escape. The first one is thermal energy provided at the surface by high equilibrium temperatures. It is possible for planets with low gravitational potentials and high equilibrium temperatures to have atmospheres that are flowing off the planet from the planetary surface. In this cases the thermal energy of the gas at the surface is already high enough to overcome the gravitational attraction of the planet and the particles reach escape velocities as they expand upwards from the surface, transforming thermal energy to kinetic energy. This form of hydrodynamic escape is called *boil off* and can lead to extremely high atmospheric escape rates. It needs no additional heating source and is described for example in Volkov and Johnson [2013], Erkaev et al. [2015], Lammer et al. [2016] and Owen and Wu [2016].

The second possibility is the absorption of large amounts of thermal energy higher

up in the atmosphere. Examples for such input sources are stellar XUV radiation or catastrophic events like planetesimal collisions. The absorbed thermal energy heats the particles in a certain layer of the gas. They again expand upwards, which accelerates them further until they reach escape velocity. This form of hydrodynamic escape is called *blow off*. Hydrodynamic escape due to external heating sources is orders of magnitudes less effective as hydrodynamic escape driven by the planets equilibrium temperature. This is mainly due to the fact that in the case of an external heating source, the additional energy is provided much higher in the atmosphere, where lower particle densities lead to smaller particle escape rates. Basically not the whole atmosphere, but only the part at and above the absorption layer has a high enough thermal energy to flow of the planet [Catling and Zahnle, 2009; Lammer, 2013].

2.2.2 Non-thermal escape processes

Particle escape can also occur due to non-thermal mechanisms that give single particles enough energy to reach escape velocity. The important difference to thermal processes is that much smaller input energies are needed, as the additional energy is not used to heat the whole gas but is focused on a single particle [Bauer and Lammer, 2004; Catling and Zahnle, 2009; Coates, 2010].

Charge exchange

There are two cases of the charge exchange process. In the first case a fast ion of the stellar wind interacts with a neutral atmospheric particle by exchanging its charge. The formerly neutral particle is ionized and accelerated and trapped within the magnetosphere. It can then recombine with an electron, giving the now again neutral particle enough energy to escape. In the second case a fast ion that is initially trapped in the magnetic field of the planet, interacts with a slow neutral by exchanging the charge. The previously magnetically trapped fast ion is now a fast neutral and able to escape from the system. The resulting slow ion is trapped in the magnetic field [Bauer and Lammer, 2004; Catling and Zahnle, 2009; Coates, 2010].

Sputtering

Fast ions impact on the atmosphere and can knock out atoms in a process called sputtering. The sources of these fast particles for example can be a stellar wind or particles trapped in a radiation belt. They collide with one of the atmospheric particles, transferring enough kinetic energy for the particle to escape [Bauer and Lammer, 2004; Catling and Zahnle, 2009; Coates, 2010].

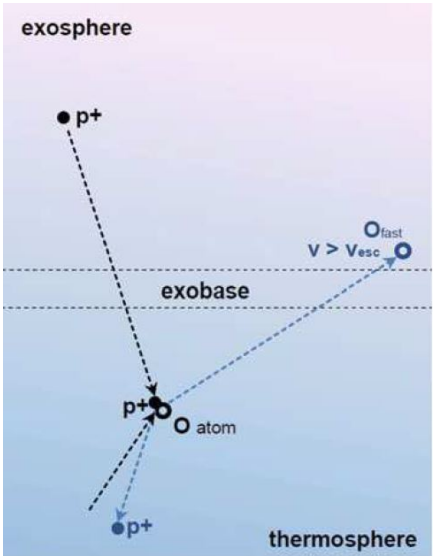

Figure 5: Illustration of the sputtering process. A fast ion collides with a slow atmospheric particle energizing it enough to escape [Lammer, 2013]

.

Photochemical reactions

Photochemical reactions are reactions of atmospheric species with ultraviolet or X-ray photons. The atmospheric particles absorb the photons and their energy. These interactions lead to photoionization and -dissociation. In the case of photoionization additional ions are produced, trapped in the magnetosphere and can then recombine with electrons, giving the newly formed neutral particle enough energy to escape. Photodissociation on the other hand breaks bigger molecules apart into smaller components and provides them with additional energy [Bauer and Lammer, 2004; Catling and Zahnle, 2009; Coates, 2010].

Ion escape

In the polar regions ions flow upwards along the field lines and then downwards towards the magnetotail. Through plasma interactions between ions and electrons the particles can gain additional energy. Since the electrons have a much higher thermal velocity, they can easily escape, setting up an electric field by charge seperation that moves the ions upwards after the electrons [Bauer and Lammer, 2004; Catling and Zahnle, 2009; Coates, 2010].

Ion pickup

At planets with no intrinsic magnetic field, like Mars and Venus, the exobase is above the interaction region of the stellar wind with the planet. In case a particle in this region becomes photoionized, it can be picked up by the stellar wind flow. The additional energy needed to escape is hereby provided by the electric field of the stellar wind [Bauer and Lammer, 2004; Catling and Zahnle, 2009; Coates, 2010].

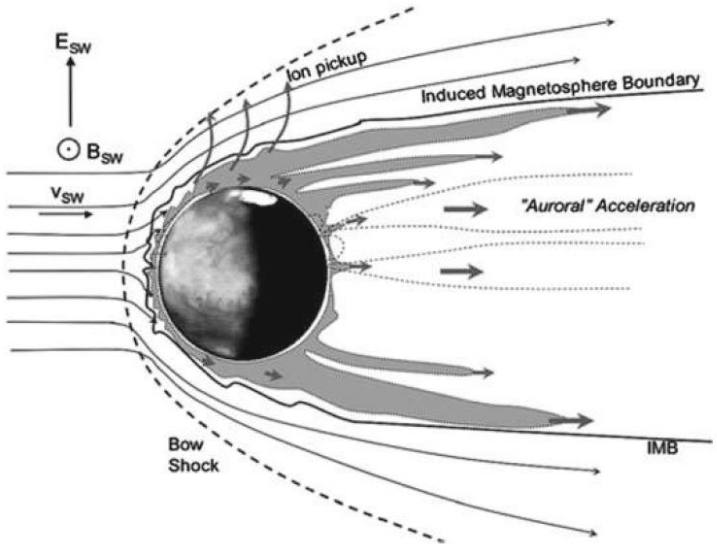

Figure 6: Illustration of ion pickup process at an un- or weakly magnatized planet. Ions are picked up above the planet because of stellar wind interactions and are accelerated by electric fields throughout the tail [Lammer, 2013]

.

2.2.3 Dominant escape process

All of the above mentioned processes can lead to particle escape from a planetary atmosphere and to calculate the exact escape rate one would need to account for all these mechanisms. When trying to quantify the flux of particles lost, it is therefore important to determine which process dominates the escape. This may vary from planet to planet. One planet might be dominated by Jeans escape while a different one, due to the lack of a magnetic field, is dominated by exosphere/solar-wind interactions. Watson et al. [1981] specifically state in their paper that they want to quantify the particle escape in a system that is dominated by hydrodynamic escape. They even specify that the majority of the input energy is supposed to be supplied by the absorption of XUV radiation in the atmosphere.

It is therefore important to notice that all of their considerations, assumptions and mathematical descriptions only apply to systems that are dominated by XUV driven hydrodynamic escape. Planets where non-thermal processes become non-negligible, where very high equilibrium temperatures are already sufficient to cause significant hydrodynamic escape without an external heating source (*boil off*) or where the thermal energy input is low enough that hydrodynamic and Jean's escape are of the same magnitude can not be described with their energy-limited escape formalism [Watson et al., 1981].

2.3 Derivation of the energy-limited escape formalism

2.3.1 The setup

After specifying the system they want to describe, Watson et al. [1981] continue to derive a mathematical model to quantify the particle loss rate of such a system. To set up their mathematical model, they make the following assumptions:

- The energy is supplied by XUV radiation at a rate S with $[S] = \frac{J}{m^2 s}$, which has already been suitably averaged over a sphere.
- The less-than-unity efficiency of XUV heating, which corresponds to the fact that not all of the incident XUV radiation is used to thermally heat the gas, is already accounted for in S. This means that S is the total energy input flux that is used to drive hydrodynamic escape.
- The photospheric radius of the planet shall be r_0.
- The XUV radiation is mostly absorbed in a narrow region near r_1, the level where the optical depth of the atmosphere to XUV is unity.

Using this setup one can equate the energy input to the energy of escape, which yields [Watson et al., 1981]:

$$F = \frac{S r_1^2 r_0}{GMm} \tag{3}$$

where F is the particle escape flux in particles per steradian and second, G is the gravitational constant, M is the mass of the planet and m is the mass of the particle. Watson et al. [1981] continue to outline the main difficulty of the model:

> "An upper limit to the escape rate is thus immediately obtained, provided the value of r_1 can be specified. However fixing r_1 is not such a simple matter." [Watson et al., 1981]

In order to quantify the escape rate, it is therefore important to determine r_1. The rest of the derivation is an attempt to derive a mathematical model that allows for the simultaneous calculation of the escape flux and r_1.

2.3.2 The model description and its assumptions

In order to mathematically describe the gas Watson et al. [1981] make the following assumptions:

- The gas is dynamically expanding
- The gas is non-viscous
- The gas has a constant molecular weight
- The pressure in the gas is isotropic

This allows for the setup of the steady-state hydrodynamic equations of mass, momentum and energy conservation [Watson et al., 1981]:

$$\vec{\nabla} \cdot (n\vec{u}) = 0 \tag{4}$$

$$mn(\vec{u} \cdot \vec{\nabla})\vec{u} + \vec{\nabla}(nkT) = nm\vec{g} \tag{5}$$

$$\vec{\nabla}(\kappa\vec{\nabla}T) = \vec{\nabla} \cdot \left(\frac{5}{2}nkT\vec{u} + n\frac{mu^2}{2}\vec{u}\right) - nm\vec{g} \cdot \vec{u} - q \tag{6}$$

where $\vec{u}$ is the bulk velocity of the gas, $\vec{g}$ is the gravitational acceleration, κ is the thermal conductivity and q is the volume heating rate. Watson et al. [1981] continue to introduce dimensionless variables for temperature, velocity and position by using an arbitrary reference temperature T_0:

$$\tau = \frac{T}{T_0} \tag{7}$$

$$\Psi = \frac{mu^2}{kT_0} \tag{8}$$

$$\lambda = \frac{GMm}{kT_0 r} \tag{9}$$

The dimensionless position variable λ corresponds to the Jeans parameter that governs Jeans escape (see section 2.2.2). Using the planetary radius as r and equilibrium temperature as T_0 λ corresponds to the restricted Jeans parameter introduced by Fossati et al. [2017]. They also parameterize the thermal conductivity of a neutral gas as [Watson et al., 1981]:

$$\kappa = \kappa_0 \tau^{0.7} \tag{10}$$

Equations 4, 5 and 6 can be mathematically reduced to two differential equations [Watson et al., 1981]:

$$\left(1 - \frac{\tau}{\Psi}\right) \frac{d\Psi}{d\lambda} = 2\left(1 - \frac{2\tau}{\lambda} - \frac{d\tau}{d\lambda}\right) \tag{11}$$

$$\frac{\kappa_0 GMm}{k^2 T_0 F} \tau^{0.7} \frac{d\tau}{d\lambda} = \epsilon + \lambda - \frac{5\tau}{2} - \frac{\Psi}{2} \tag{12}$$

where ϵ is the energy each escaping particle carries away from the system and is defined as [Watson et al., 1981]:

$$\epsilon = \epsilon_\infty - \frac{1}{FkT_0} \int_r^\infty q r^2 dr \tag{13}$$

where ϵ_∞ denotes the energy flow at infinity. In the special case where $\epsilon_\infty = 0$, the energy flowing outward is just enough to lift the gas from the gravitational field, but does not leave any access energy at very large distances. Watson et al. [1981] argue later that they always assume that this is the case for every escaping particle, since any additional energy carried away would only decrease the maximum particle escape flux. ϵ_∞ is therefore neglected in the further derivation. To further simplify these equations Watson et al. [1981] make a variety of additional assumptions at this point:

- They define a lower boundary λ_0 somewhere above the homopause, where the temperature is fixed at T_0 ($\tau(\lambda_0) = 1$).
- Above the lower boundary the mixing ratios of heavier gases are much smaller than that of hydrogen, making hydrogen the dominant gas everywhere above it.
- The atmosphere at the lower boundary is treated as "tightly bound", meaning that the gravitational attraction of the planet at this level is still sufficient to keep an atmosphere with the corresponding temperature T_0 from escaping catastrophically. This implies that the thermal velocity at the lower boundary

must be small compared to the gravitational escape velocity. The tightly bound condition is met if $\lambda_0 \gtrsim 10$ [Parker, 1964].

- The optical depth to XUV radiation at the lower boundary is much greater than one.
- All the XUV radiation is absorbed in a narrow region at r_1. The optical depth to XUV at this level is unity.
- The pressure at large distances declines toward zero.

Finally Watson et al. [1981] introduce their "subsonic" assumption. The "sonic level" r_s is defined as the level where the velocity passes smoothly from subsonic ($\Psi < \tau$) to supersonic ($\Psi > \tau$) flow. The level of XUV absorption r_1 is then assumed to be below the sonic level:

$$r_1 < r_s \tag{14}$$

In the appendix of Watson et al. [1981] the authors show that this assumption implies:

$$\frac{\lambda_1}{\tau_1} > 2 \tag{15}$$

This condition in turn allows to place limits on the temperatures in the thermosphere and greatly simplifies the mathematical treatment of the differential equations [Watson et al., 1981].

2.3.3 The temperature profile and its limiting condition

To continue their derivation and use all these assumptions Watson et al. [1981] introduce the following dimensionless variables for particle escape flux and XUV heating:

$$\zeta = F \cdot \frac{k^2 T_0}{\kappa_0 G M m} \tag{16}$$

$$\beta = S \cdot \frac{G M m}{k T_0^2 \kappa_0} \tag{17}$$

While ζ simply denotes the particle escape flux, β is called the energy parameter and contains system parameters like XUV flux, mass of the planet and lower boundary temperature. Equation 12 for the region below r_1 can then be rewritten as [Watson et al., 1981]:

$$\frac{\tau^{0.7}}{\zeta}\frac{d\tau}{d\lambda} = \lambda - \frac{\beta}{\zeta\lambda_1^2} - \frac{5\tau}{2} - \frac{\Psi}{2} \tag{18}$$

The authors continue to argue:

> "Well below the sonic level, the velocity term is negligible. Near the lower boundary, $\lambda >> \tau$ from our first assumption, so the equation may be further simplified:" [Watson et al., 1981]

$$\frac{\tau^{0.7}}{\zeta}\frac{d\tau}{d\lambda} = \lambda - \frac{\beta}{\zeta\lambda_1^2} \tag{19}$$

This is an approximate differential equation of the temperature profile τ with regard to change in height λ. In order to understand this equation, it is important to understand what is physically happening in the thermosphere. At the lower boundary there is a fixed temperature T_0, which is also the reference temperature for the dimensionless temperature profile τ. Let us start by imagining a system with no XUV heating. In this case, the atmosphere, which is expanding outwards, cools adiabatically and the temperature drops monotonically from the lower boundary to higher levels. It is important to keep in mind that the atmosphere would strictly cool with height, due to adiabatic cooling, in the absences of absorbed XUV energy. The atmosphere would still expand driven by the thermal energy input from the planet, but the expansion would be slow and the atmospheric escape would be limited to Jeans escape [Watson et al., 1981].

When XUV energy is added to the system, the picture changes. The temperature profile takes different shapes, depending on how the added XUV energy is used. Some of the energy is used to drive escape, giving particles traveling in the right direction the additional energy needed to escape. However, a portion of the absorbed energy is also conducted downwards and heats the lower parts of the atmosphere. In case the escape flux ζ is low, the majority of the energy is conducted towards the lower boundary and is used to heat the lower part of the thermosphere. In this case the temperature increases monotonically from the lower boundary on to the absorption height λ_1. Such a case is depicted in the curve denoted "A" in Figure 7 [Watson et al., 1981].

If the escape flux ζ however increases, most of the energy is used to drive particle escape and there is not enough energy left to conduct downwards, to counteract adiabatic cooling at the lower boundary. As can be seen in the temperature profile denoted "B" in Figure 7, the temperature in this case first starts to drop, until at

one point there is enough energy conducted from the absorption layer to counteract adiabatic cooling and reheat the atmosphere [Watson et al., 1981].

It becomes obvious that the escape rate ζ may not increase infinitely. With increasing ζ the minimum in the temperature profile increasingly steepens until at one point so much energy would go into escape, and so less energy into heating of the lower atmosphere that a negative temperature would be reached in the profile. A negative temperature is of course physically unreasonable, therefore placing a limit on how high ζ may get for any given system [Watson et al., 1981].

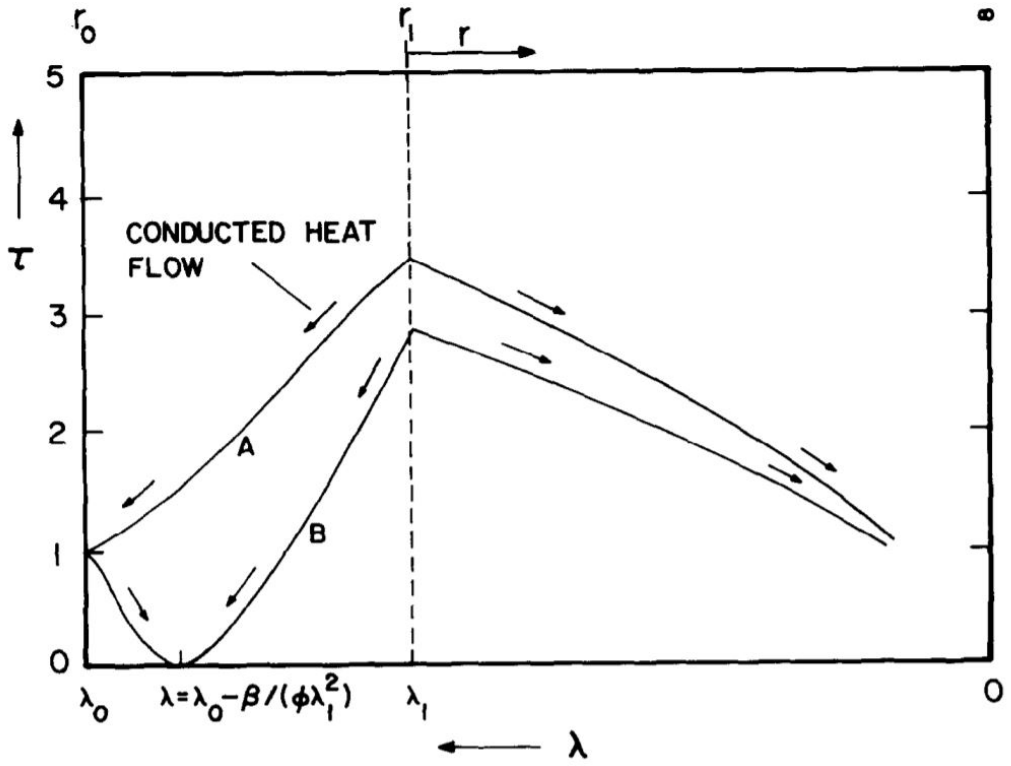

Figure 7: Temperature profiles τ of two thermospheres with the same fixed lower boundary λ_0 and which absorb XUV energy at λ_1. The line denoted "A" depicts a scenario with a low escape rate, where most of the absorbed energy is used to heat the lower parts of the atmosphere. The line denoted "B" depicts a scenario with a high escape rate, where not enough energy is conducted downwards to counteract adiabatic cooling at the lower boundary [Watson et al., 1981].

2.3.4 The solution

Watson et al. [1981] are interested in this special case, where the escape rate is just low enough to still allow for positive temperatures in the temperature profile of the thermosphere. They use the fact that in this special case both τ and $\frac{d\tau}{d\lambda}$ must be zero to obtain a set of equations for the energy-limited flux and the height of the XUV absorption level. The exact derivation is depicted in the appendix of Watson et al. [1981].

$$\zeta_m = \frac{2}{1.7}\left[\frac{\left(\frac{\lambda_1}{2}\right)^{\frac{1.7}{2}}+1}{\lambda_0-\lambda_1}\right]^2 \tag{20}$$

$$\lambda_1 = \sqrt{\frac{\beta}{\zeta_m}\left[\lambda_0 - \sqrt{\frac{2}{1.7\zeta_m}} + \epsilon_\infty\right]^{-1}} \tag{21}$$

This system of equations is known as the energy-limited escape formalism and provides a solution for both the maximum escape flux ζ_m as well as the height of the absorption level λ_1 given a specific planetary system. The equations will yield a solution no matter whether the system complies with all the assumptions used within the derivation or not. That means every system, where this formalism is applied, must first be thoroughly checked whether or not it fulfills all the parameters required by the assumptions. Also note that the solution aims to overestimate the maximum escape flux and therefore provides an upper limit for it.

2.4 Escape rates obtained with energy-limited approaches

When examining the derivation of the energy-limited escape formalism in Watson et al. [1981] closely, one finds that there are actually two different mass-loss rates that can be obtained with the energy-limited approach. Both equation 3 and 16 claim to state the particle escape flux F. However, the two equations do not equate:

$$\frac{SGMmr_0}{k^2T_0^2\lambda_1^2} \neq \frac{\frac{2}{1.7}\left[\frac{\left(\frac{\lambda_1}{2}\right)^{\frac{1.7}{2}}+1}{\lambda_0-\lambda_1}\right]^2 \kappa_0 GMm}{k^2T_0} \tag{22}$$

Equation 3 is derived from the principal of energy conservation and does not use any assumptions, however must be provided with an estimate of the XUV absorption

height r_1. Equation 16 on the other hand is a consequence of the simplifications and approximations used in the derivation of the energy-limited equations. Therefore after numerically solving the energy-limited equations one may choose how to calculate the corresponding particle escape rate.

Escape rate based on the solution ζ

Using equation 16 one can obtain an energy-limited particle escape rate:

$$F_\zeta = \frac{\zeta \kappa_0 GMm}{k^2 T_0} \tag{23}$$

Particle escape rates and corresponding mass-loss rates obtained with this relation will be denoted with the subscript ζ from here on.

Escape rate based on the solution λ_1

Using equation 3 one can obtain an energy-limited particle escape rate:

$$F_{\lambda_1} = \frac{SGMmr_0}{k^2 T_0^2 \lambda_1^2} \tag{24}$$

Particle escape rates and corresponding mass-loss rates obtained with this relation will be denoted with the subscript λ_1 from here on.

Escape rate based on $r_1 = r_0$

There is actually a third way the energy-limited approach is sometimes used. To avoid the problem of fixing r_1 some studies simply set $r_1 = r_0$ and use equation 3 again to obtain an energy-limited particle escape rate by setting r_0 equal to the planetary radius R_{pl}:

$$F_{R_{pl}} = \frac{SR_{pl}^3}{GMm} \tag{25}$$

Particle escape rates and corresponding mass-loss rates obtained with this relation will be denoted with the subscript R_{pl} from here on.

All three methods of obtaining a particle escape rate including their differences will be investigated more in detail in chapter 6.

2.5 Application to the evolution of Earth and Venus

Equations 20 and 21 are the main result of Watson et al. [1981]. The rest of the paper focuses on applying the formalism to the evolution of Earth and Venus. They calculate possible escape rates and discuss the possibility of more massive volatiles being dragged along with the escaping hydrogen particles. They conclude that the calculated escape rates are not able to explain the observed isotope ratios of heavier volatiles on the terrestrial planets of the solar system [Watson et al., 1981].

2.6 Roche lobe effect

Erkaev et al. [2007] have improved the energy-limited approach slightly in 2007, where it otherwise has been mostly unaltered since its first introduction. Their formulation includes a simple averaging constant for the incident XUV flux of $\frac{1}{4}$. They argue that the total amount of energy supplied is only dependent on the cross-section of the stellar radiation and the planetary atmosphere, which is πr_1^2. The distribution of the energy on the other hand is averaged over the whole surface of the sphere $4\pi r_1^2$. The ratio of cross-section to surface area corresponds to the averaging factor $\frac{1}{4}$ [Erkaev et al., 2007].

The more important contribution to the energy-limited approach by Erkaev et al. [2007] however, was the consideration of the Roche lobe effect. The Roche lobe is the region around a planetary body in which the particles within this region are gravitational bound to the planet. At the Roche lobe the gravitational attraction of the planet is exactly equal to the gravitational attraction of the host star. In the case of atmospheric escape this means that particles do not necessarily need to acquire escape velocity, but its enough for them to reach the Roche radius in order to escape the gravitational attraction of the planet. This results in an increase of the particle escape rate, which is represented by a correction factor K [Erkaev et al., 2007].

$$K = 1 - \frac{3R_{pl}}{R_{Rl}} + \frac{R_{pl}^3}{2R_{Rl}^3} \tag{26}$$

with the Roche radius R_{Rl} and the planetary radius R_{pl}:

$$R_{Rl} \approx d \left(\frac{M_{pl}}{3M_{star}} \right)^{\frac{1}{3}} \tag{27}$$

where d is the orbital separation of the star and the planet, M_{pl} is the planetary mass and M_{star} is the stellar mass.

The Erkaev et al. [2007] formulation of the energy-limited approach is the nowadays used formulation of the approach and usually is stated as the mass-loss rate $\dot{M}\left[\frac{kg}{s}\right]$ instead of the particle escape rate $F\left[\frac{1}{sr \cdot s}\right]$:

$$\dot{M} = \frac{\pi \Phi_{XUV} R_{XUV}^2 R_{pl}}{GMK} \tag{28}$$

where Φ_{XUV} is the total incidend stellar XUV flux, $R_{XUV} = r_1$ is the effective radius of XUV absorption and $R_{pl} = r_0$ is the planetary radius.

3 Investigation of the validity of the assumptions

In this chapter the different assumptions used in Watson et al. [1981] and mentioned in the previous chapter are being investigated more in detail. Their validity is checked and possible limitations on the applicability of the energy-limited escape formalism in different systems are being pointed out.

3.1 The presence of a large hydrogen envelope

The authors first assumption is that the planetary body under investigation has accumulated an extensive hydrogen envelope during its formation within the solar nebula. This assumption has already been discussed in great detail in section 2.1. This discussion concluded that in order for this to happen the planet needs to follow a fast accretion evolution track and accumulate a mass of a few tenth of an Earth mass within the first 10 Myrs of its evolution. It was also already discussed in the same section that there is significant evidence for the possibility of such an evolutionary track, although until today it is still highly debated which planetary formation scenario is the most likely.

3.2 Hydrodynamic escape as dominant escape process and stellar XUV history

Watson et al. [1981] continue by specifying that in their system under consideration, hydrodynamic escape must be the dominant escape process and all other escape mechanisms must be negligible compared to it. A detailed discussion of the different escape mechanisms was provided in section 2.2 and concludes that for hydrodynamic escape to be dominant, the atmosphere must be strongly heated. The most common source of such heating is the absorption of stellar XUV radiation in the atmosphere [Yelle, 2004; Catling and Zahnle, 2009; Erkaev et al., 2013]. Present solar XUV fluxes are at an order of magnitude of about $10^{-2}\frac{J}{m^2 s}$. Watson et al. [1981] have shown that such values would be able to remove a significant amount of hydrogen over the course of a planet's evolution (for example about $5.5 \cdot 10^{-5}$ Earth masses in the first 600 Myrs of Earth's history). However, they also showed that the escape would not be sufficient to remove enough heavier elements to explain present day isotope ratios in the atmospheres of the terrestrial planets of our solar system. Compared with planetary evolution theories, like the "modified homogeneous accretion theory", which require for a large amount of volatiles to be removed, hydrodynamic escape can only account for about 10% of the loss rate. Therefore it is highly doubtful whether hydrodynamic escape would really be significantly more dominant than other escape mechanisms under such conditions [Watson et al., 1981]. A period of dominant hydrodynamic es-

cape might only have existed in the early stages of the planets evolution, when it was still accreting mass and therefore had a lower mass than present day earth. Lammer et al. [2020] have shown that removing volatiles from a proto-Earth with a mass of for example 0.55 Earth masses is much more efficient than from present-day earth.

Research in the almost 40 years since the publication of Watson et al. [1981] has profoundly changed this picture. In order to gather clues on the possible evolution of our own solar system astronomers have looked closely at a variety of Sun-like stars in our cosmic neighborhood. They have found that the rotation rate of a star, hence its magnetic activity, decays over time. A higher magnetic activity means also more chromospheric emission, which in turn means a higher XUV luminosity. In detail the studies have found the following results [Tu et al., 2015]:

- The rotation rate and the correlated XUV luminosity of a solar-like star decays with time, resulting in younger stars having between 10^2 and 10^3 higher XUV luminosities than our Sun today.
- There is a saturation threshold for the possible X-ray luminosity at about 0.001 of the bolometric luminosity of the star. This means that for all solar-like stars with a rotation period of only a couple days or less, the XUV luminosity is roughly the same.
- Depending on the original rotation period, the solar-like stars are being divided into three groups: Fast rotators, intermediate rotators and slow rotators. The observed rotation periods are continuous and the three categories merge at their respective boundaries. As can be expected fast rotators stay much longer on the saturated XUV luminosity level than moderate rotators, which in turn again stay there longer than slow rotators.
- After about 3 Gyrs all three paths converge again, making it practically impossible to determine the type of rotator from present day observations.

To illustrate the above mentioned points Figure 8 shows the different evolutionary tracks of the XUV luminosity for all three types of rotators [Lammer et al., 2018].

A subsequent investigation of the isotope ratios in Earth's and Venus' atmosphere and soil by Lammer et al. [2020] narrowed the possible rotation tracks of our Sun down and was able to exclude the possibility of a fast rotator. They found that the young Sun was somewhere between a slowly and moderatly rotating star.

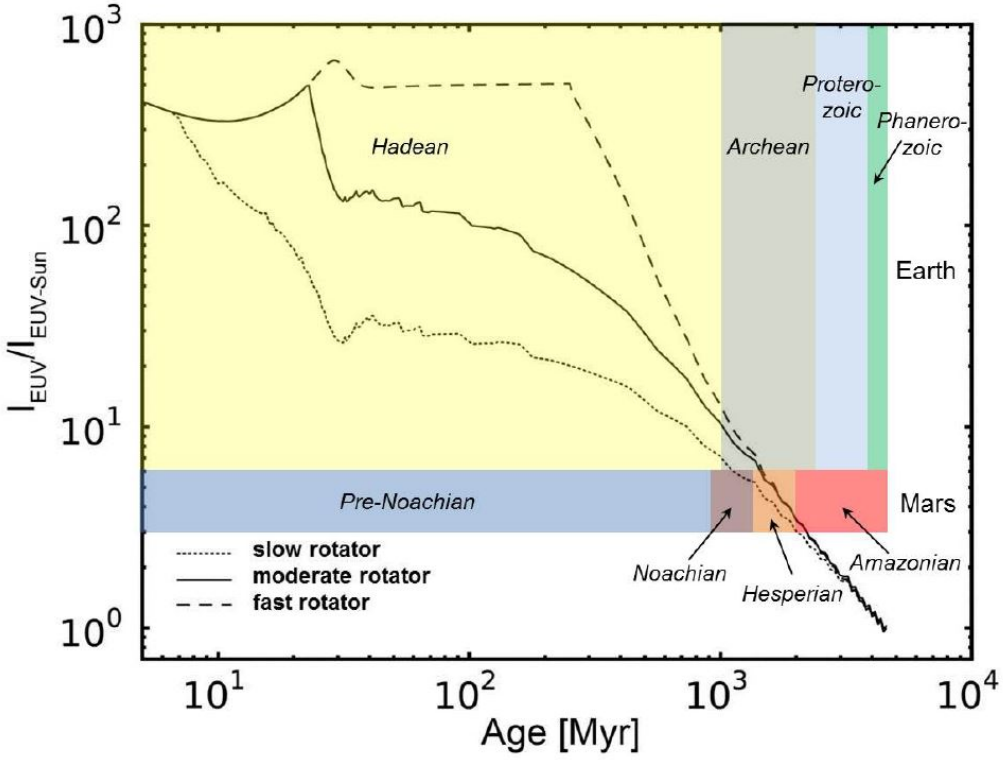

Figure 8: Expected ratio of XUV luminosity to the present day solar value for Sun-like stars over the course of their evolution. The dotted line represents a slowly rotating star, the solid line a moderately rotating star and the dashed line a fast rotating star. The color shaded areas represent different archeological times on Earth and Mars. The data was produced by Tu et al. [2015] and the Figure published in Lammer et al. [2018].

In conclusion, the present day solar XUV luminosity is not high enough to make hydrodynamic escape the dominant escape process in a hydrogen dominated young atmosphere. It certainly would not be able to remove a significant amount of more massive volatiles. However, studies of solar-like stars have shown that the XUV luminosity of younger stars is much higher, even making values of 400 times the present day value for a period of a few hundreds of Myrs possible. This greatly increased XUV luminosity in the early days of the stellar systems evolution justifies neglecting all other escape processes and assuming hydrodynamic escape to be the dominant escape process.

Finally it is important to again emphasize the main limitation this assumption implies: If one wants to accurately describe the order of magnitude of the overall particle

escape on a planetary system, the energy-limited escape formalism may only be used, if the systems particle escape is dominated by hydrodynamic escape. All other forms of escape, especially non-thermal escape mechanisms, must be negligible.

3.3 Parameterization of energy supply by XUV heating

To supply XUV energy to the system, Watson et al. [1981] use the parameter S. They also state that "S is already suitably averaged over a sphere and corrected for the less-than-unity efficiecy of XUV heating". S denotes the energy that is absorbed per second and square meter and which then is used to thermally heat the gas in order to drive hydrodynamic escape. The fact that the amount of energy supplied by the host star is not constant over time is irrelevant, as the energy-limited escape formalism anyway only provides an escape flux value for a specific moment in which a specific amount of energy is supplied. The averaging over a sphere is needed, as only those parts of the atmosphere facing the host star can actually absorb XUV energy and their absorption also differs depending on the incident angle. However, since the planet spins and thermal conduction and convection to some extend transfer some of the absorbed energy, the heating can be averaged over the whole sphere. To justify this assumption, it is important to note that hydrodynamic escape is a continuous process. Not one single absorption event leads to the escape of one particle, but the sum of all the absorption events leads to a heating of the gas in the absorption region, which in turn allows for the gas to flow upwards and escape. Therefore hydrodynamic escape also happens on the night side as the atmosphere still retains some of its heat. Of course in any given moment the dayside escape flux will be higher than the nightside one, but it is reasonable to average the energy input over the whole system and therefore also to aim for an averaged escape flux of the whole system, since only with an averaged value an evolution over time can be investigated. The averaging can be achieved by simply taking a quarter of the incident total stellar XUV flux Φ_{XUV} at the orbital distance of the planet as the ratio of the cross-section area of the planet πr^2 and its surface area $4\pi r^2$ is equal to $\frac{1}{4}$ [Erkaev et al., 2007; Catling and Zahnle, 2009; Coates, 2010].

On the account of the less-than-unity efficiency of XUV heating, Watson et al. [1981] have made their formalism really general. Most of the energy supplied by XUV radiation is not used to heat the absorption region, but is used in different photochemical reactions. However, it is not trivial to determine how much of the absorbed energy in a given atmosphere is actually used to drive hydrodynamic escape. Numerical simulations by Salz et al. [2016] have determined it to be roughly 20% for most planets, but have found it to decrease by several orders of magnitude once the gravitational potential of the system gets high. This phenomenon has to be accounted for in possible applications of the energy-limited escape formalism. Watson et al. [1981] were

well aware of this less-than-unity efficiency of XUV heating but did not require any assumptions about it in their derivation. They simply said it to be already accounted for in the parameter S, making it equivalent to the total energy input to the whole atmosphere that is actually used to drive hydrodynamic escape. Every user of the formalism may then define for themselves how large S actually is.

To sum up, the definition of the energy-input parameter S does not pose any limitations on the applicability of the formalism. However, it must be noted that it is crucial to carefully consider the correct value of S, especially the efficiency of XUV heating hidden within it.

3.4 Absorption in a narrow region

In order to supply the XUV energy to the atmosphere, Watson et al. [1981] assume all of it to be absorbed in a narrow region near the level r_1, which is defined as the level, where the optical depth of the atmosphere to XUV is one. It is obvious that not all of the energy is actually absorbed just at a level r_1. However it seems reasonable to assume that a majority of it is. The optical depth τ_{od} is defined as the natural logarithm of the incident radiation flux Φ_i to the transmitted radiation flux Φ_t [Kitchin, 1987]:

$$\tau_{od} = ln\left(\frac{\Phi_i}{\Phi_t}\right) \tag{29}$$

This definition states that at the level where $\tau_{od} = 1$, the transmitted flux has been reduced by a factor of $\frac{1}{e}$ compared to the incident flux. The law is logarithmic, meaning that the value of the transmitted flux drops exponentially with increasing optical depth. This implies that in regions with a very low optical depth, far below 1, practically no radiation is absorbed, while in regions with an optical depth above 1 the vast majority of radiation has already been absorbed [Kitchin, 1987].

While this assumption therefore seems reasonable and justified it is however not trivial to determine the correct absorption profile of an arbitrary atmosphere. The optical depth of the medium must not increase linearly, but could increase and decrease several times on the way trough the atmosphere, depending on atmospheric conditions like density and temperature. This could result in two different levels, where the optical depth reaches close to 1 and the majority of radiation is absorbed. Tian et al. [2005] in addition have shown in simulations that due to the dependence of the optical depth to wavelength, the XUV absorption regions of planetary atmospheres can be much broader. Thermal conduction will still to some extend distribute the energy even if absorbed lower in the atmosphere. Also an averaging of the absorbed energy in the region near r_1 will still account for all the incident energy and give an

approximate value, but it is difficult to quantify exactly how much the results are changed by this simplification.

To summarize, while the assumption is certainly physically reasonable and may very well be justified in a lot of systems, especially simple hydrogen atmospheres like those under consideration, there may very well be systems with broader absorption regions and several absorption peaks. It is not trivial to describe the effects this would have on the distribution of the heating energy and the reproduction of real absorption profiles for XUV in hydrogen atmospheres can not be easily generalized. In order to validate this assumption, one therefore has to compare the results of the energy-limited escape formalism with results obtained via a different method. This will be conducted in chapter 7 by using results from one-dimensional hydrodynamic simulations and will give a better insight on the range of applicability of the energy-limited escape formalism.

3.5 Gas properties

In order to set up their mathematical model Watson et al. [1981] assume the gas to be non-viscous, for it to have a constant molecular weight and for the pressure in the gas to be isotropic. These assumptions are easily justifiable, if one considers the low density in the thermosphere. The pressure, and therefore the particle density in an atmosphere, drops exponentially with increasing height. Therefore the pressure is already very low in its upper parts, where XUV absorption happens. To give some context, while on present day Earth the local scale height, which indicates a decrease of the atmospheric pressure by a value of $\frac{1}{e}$, is of about 8 km, the absorption height in these hydrogen atmospheres is usually of the order of few hundred to thousand kilometers above the planets surface. The non-viscous assumption is therefore justified, as the density is so low that the gas particles rarely interact with each other. The constant molecular weight assumption is also justified, as we consider a region where hydrogen is by far the dominant species in the atmosphere, therefore allowing to neglect all other species. Finally, the pressure may also be assumed to be isotropic, as it is already so low that significant disturbances within the region under investigation do not change the absolute pressure value significantly.

3.6 Energy and pressure at infinity

The mathematical description by Watson et al. [1981] also allows for the consideration of additional energy to be carried away by each escaping particle. It has already been discussed in section 2.3.2 that this would only lead to a decrease of the escape flux. Therefore neglecting it is justified as long as one aims to only provide an upper limit to the escape flux as the authors did. A similar argument can be made for the

assumption that the pressure at infinity declines towards zero. Watson et al. [1981] justify this in the appendix of their paper:

> "In reality the pressure at large distances is set by conditions in the interplanetary medium. However, the effect of nonzero pressures at infinity can only be to slow the escape of the gas. Since our purpose is to obtain upper limits for the escape, the assumption does not affect the validity of the results." [Watson et al., 1981]

3.7 Lower boundary properties

The lower boundary, which provides a fixed reference value for the temperature profile, must satisfy a variety of conditions. First hydrogen must be the dominant gas, which is certainly justified in a hydrogen envelope at a level as described in the definition of the lower boundary, well above the homopause [Watson et al., 1981].

The optical depth to XUV radiation at the lower boundary must be much greater than one. This does not put any new constraints on the formalism as we have already established that only systems with a narrow and clearly defined absorption region justify the narrow absorption region assumption. Such an absorption region must be well above the lower boundary per definition, justifying therefore also this assumption.

Finally and most importantly, the lower boundary is treated as "tightly bound". The terminology of a "tightly bound" atmosphere was first established by Parker [1964] and originally defines the thermal velocity of the gas at a specific level in the solar corona to be significantly below the gravitational escape velocity at this level. The magneto-hydrodynamic approach used to describe the solar corona can also be used to describe the gas in a planetary hydrogen atmosphere. The parameter λ_0 describes the gravitational potential and the thermal energy at the lower boundary level r_0 [Chamberlain, 1963; Watson et al., 1981]:

$$\lambda_0 = \frac{GMm}{kT_0 r_0} \tag{30}$$

Parker [1964] have shown that if this parameter is above a value of 10, the condition of a "tightly bound" atmosphere is met, the gas at the lower boundary is quasi-static and expands from there out to space reaching supersonic velocities somewhere above this level. If however $\lambda_0 \lesssim 10$, the thermal velocity is similar to or above the escape velocity, leading to a supersonic catastrophic escape at the lower boundary, which therefore invalidates its role as a reference level for the escape. The tightly bound condition therefore constraints the λ_0 parameter at the lower boundary:

$$\lambda_0 \gtrsim 10 \tag{31}$$

This is also in accordance with a much more recent study by Volkov et al. [2011] that states that for values of $\lambda_0 < 6$ escape rates start to differ sufficiently from Jeans escape and reach catastrophic escape at values of $\lambda_0 < 2.4$. The tightly-bound condition used by Watson et al. [1981] is therefore more conservative than the Volkov et al. [2011] results and validates the application of the energy-limited formalism in systems that comply with condition equation 31.

3.8 Subsonic assumption

The last assumption used in the derivation of the energy-limited escape formalism is the subsonic assumption, which states that the level of XUV absorption r_1 must be below the sonic level r_s:

$$r_1 < r_s \tag{32}$$

This assumption significantly simplifies the differential equations used in the derivation. Watson et al. [1981] tried to assess the validity of the assumption by limiting the bulk velocity at the XUV absorption height. As a conclusion to their assessment they find:

> "We conclude that the assumption is justified over the range of parameters utilized in the text, but that it may break down if the atmosphere is so strongly heated as to allow very high escape rates simultaneously with high temperatures in the thermosphere." [Watson et al., 1981]

Because of its importance in the derivation it is obvious that a more thorough investigation of this subsonic assumption must be conducted in order to validate the energy-limited escape formalism over a broader range of parameters, especially for systems with strong heating. This investigation is performed in the upcoming chapter.

4 Derivation of the limiting condition imposed by the subsonic assumption

The importance of the subsonic assumption to the derivation of the energy-limited escape formalism was pointed out in the previous section. This chapter aims to develop a limiting condition that allows to check for each individual planetary system whether or not it meets the assumption.

4.1 Derivation of the the temperature profile below the sonic level

To start with the derivation one needs a temperature profile, allowing to calculate the previously introduced dimensionless temperature parameter τ at an arbitrary height below the sonic level. Equation 15 in Watson et al. [1981] states:

$$\frac{\tau^s}{\zeta}\frac{d\tau}{d\lambda} = \lambda - \frac{\beta}{\zeta\lambda_1^2} + \epsilon_\infty \tag{33}$$

where $s = 0.7$ is the parametrization of the thermal conductivity of the gas and ϵ_∞ is the amount of energy carried away to infinity. As previously discussed, setting $\epsilon_\infty = 0$ can only lead to an overestimation of the escape flux ζ [Watson et al., 1981]. Therefore this term is neglected from now on.

$$\frac{\tau^s}{\zeta}\frac{d\tau}{d\lambda} = \lambda - \frac{\beta}{\zeta\lambda_1^2} \tag{34}$$

To continue this differential equation must be solved by integration. The conditions $\lambda = \lambda_0$ and $\tau = 1$ are used for the lower boundary.

$$\tau^s d\tau = \left(\lambda\zeta - \frac{\beta}{\lambda_1^2}\right)d\lambda \tag{35}$$

$$\int_1^{\tau'} \tau^s d\tau = \int_{\lambda_0}^{\lambda'} \left(\lambda\zeta - \frac{\beta}{\lambda_1^2}\right)d\lambda \tag{36}$$

$$\frac{\tau^{s+1}}{s+1}\bigg|_1^{\tau'} = \left(\frac{\lambda^2}{2}\zeta - \frac{\beta}{\lambda_1^2}\lambda\right)\bigg|_{\lambda_0}^{\lambda'} \tag{37}$$

$$\frac{\tau'^{s+1}}{s+1} - \frac{1}{s+1} = \left(\frac{\lambda'^2}{2}\zeta - \frac{\beta}{\lambda_1^2}\lambda'\right) - \left(\frac{\lambda_0^2}{2}\zeta - \frac{\beta}{\lambda_1^2}\lambda_0\right) \tag{38}$$

$$\frac{\tau'^{s+1}-1}{s+1} = \frac{\zeta}{2}\left(\lambda'^2 - \lambda_0^2\right) - \frac{\beta}{\lambda_1^2}\left(\lambda' - \lambda_0\right) \tag{39}$$

Solving for τ' yields a function for the temperature depending on the height in the atmosphere λ'. For simplicity all primed values are replaced with unprimed values:

$$\tau = \left\{1 + (s+1)\left[\frac{\zeta}{2}(\lambda^2 - \lambda_0^2) - \frac{\beta}{\lambda_1^2}(\lambda - \lambda_0)\right]\right\}^{\frac{1}{s+1}} \tag{40}$$

If the height of XUV absorption λ_1 is known or fixed, this formula can be used to investigate the escape rate dependence of the temperature profile. As long as the escape flux is below a critical value, the temperature will monotonically rise between λ_0 and λ_1. If the escape flux further increases, the remaining XUV energy, which is conducted down to the lower atmosphere, is not sufficient to counteract adiabatic cooling and a temperature minimum will appear [Watson et al., 1981].

Equation 40 analytically only describes a temperature profile, if the height of XUV absorption is known. The parameter λ_1 must be provided as input. It is also very important to note at this point that this equation is dependent on the assumption that the height of the XUV absorption is well below the sonic level. This temperature profile only allows for the calculation of a temperature at a height below the sonic level, but not above it.

4.2 Derivation of the limit of the temperature parameter

After enabling the calculation of the temperature profile, the further derivation aims to find a limiting condition for the temperature parameter τ that allows for the validation of the subsonic assumption. Watson et al. [1981] examine their subsonic assumption further in the appendix, in the section "Examination of Assumptions", sub-section a) "r_1 Lies below the Sonic Level". In this section equation A11 provides an upper limit of the dimensionless velocity parameter Ψ_1 (defined in equation 6 in Watson et al. [1981]), representing the bulk velocity at the XUV absorption height r_1:

$$\Psi_1 < \frac{m}{k^3 T_0}(\kappa_0 \tau_1 \zeta \sigma)^2 \tag{41}$$

Calculating for all the known parameters the equation yields [Watson et al., 1981]:

$$\Psi_1 < 1.2605 \frac{(\zeta \kappa_0)^2}{T_0} \tau_1^2 \tag{42}$$

It is known from the definition of the sonic level that $\Psi < \tau$ everywhere below the sonic height r_s and $\Psi > \tau$, everywhere above it. So if $\Psi < \tau$, then $r_1 < r_s$. Since the aim is to determine under which conditions the XUV absorption height lies below the sonic level, a limit for the temperature at the XUV absorption height τ_1 can be found from equation 42 [Watson et al., 1981]:

$$\tau_1 < \frac{T_0}{1.2605 \cdot (\zeta \kappa_0)^2} \tag{43}$$

With the previously derived temperature profile equation 40 the temperature at r_1 can be calculated and compared with the derived limit equation 43, as long as the subsonic assumption is valid. This means that if the assumption is valid, the above written condition must apply. However, if it is not valid, the condition may still be met, as the temperature at r_1 can not be correctly calculated.

It is crucial to understand: If the calculated temperature is above the temperature limit, the subsonic assumption is certainly violated. However, if it is below the limit, no certain conclusion on the validity of the subsonic assumption can be drawn for the particular case.

5 Planetary grid

As discussed in detail in chapter 3, the energy-limited escape formalism introduced by Watson et al. [1981] uses a large number of assumptions. The validity, at least in certain parameter ranges, of a variety of these assumptions is not certain and must be studied further. This can be performed by using numerical methods and comparing the results with results from different models. However, to do so, first a grid of theoretical planets must be defined. The grid limits determine the parameter limits of the validity investigation and the individual grid points can be used to perform numerical calculations and comparisons with other models. Therefore a grid of planets for the further investigation of the energy-limited escape formalism is defined in this chapter.

As described in chapter 7 a hydrodynamic upper atmosphere model developed by Kubyshkina et al. [2018a] is used to compare the results of the energy-limited escape formalism with the results of their model. The planetary grid defined in this chapter will therefore from here on be called "comparison-grid". Its limits will be determined mainly by the grid limits of the hydrodynamic upper atmosphere model by Kubyshkina et al. [2018a]. Their grid is limited by five different parameters:

- Stellar Mass
- XUV flux
- Equilibrium temperature
- Planetary radius
- Planetary mass

Since the energy-limited escape formalism does not care for stellar parameters, the stellar mass parameter is disregarded in the comparison-grid, using a stellar mass of one solar mass for all planets.

Kubyshkina et al. [2018a] provide in Table 3 three different EUV and X-ray luminosities for a star with a stellar mass of one solar mass. One for an inactive, one for a moderately active and one for an active star. The luminosities for an inactive and an active star are chosen as lower and upper limits for the comparison-grid. The corresponding XUV flux Φ_{XUV} is then calculated using the orbital separation d_0 of the planet. The orbital separation in turn is determined by the equilibrium temperature of the planet. Equations 44 and 45 show how the lower and upper limit for the XUV flux for a specific orbital separation d_0 are calculated.

$$\Phi_{XUV}^{min}\left[\frac{J}{m^2 s}\right] = \frac{4.7519 \cdot 10^{27}[\frac{J}{s}]}{4 \cdot \pi \cdot (d_0[m])^2} \tag{44}$$

$$\Phi_{XUV}^{max}\left[\frac{J}{m^2 s}\right] = \frac{1.6438 \cdot 10^{30}[\frac{J}{s}]}{4 \cdot \pi \cdot (d_0[m])^2} \tag{45}$$

For the comparison-grid, a set of 30 logarithmically spaced values between those limits is used for each equilibrium temperature value (determining the orbital separation). For the equilibrium temperature 18 evenly spaced values between 300 and 2000 K, for the planetary radius 10 evenly spaced values between 1 and 10 $R_\oplus$ (Earth radii) and for the planetary mass 39 evenly spaced values between 1 and 39 $M_\oplus$ (Earth masses) are chosen.

The heating efficiency ν, which determines how much of the incoming XUV flux is used to drive hydrodynamic escape, is set to be $\nu = 0.15$ for all systems in accordance with Kubyshkina et al. [2018a] and Shematovich et al. [2014]. This is also in accordance with the results of Salz et al. [2016], which showed that for planets with a very high gravitational potential Φ_G, the heating efficiency ν drops several orders of magnitude. For all planets below a certain threshold however, the heating efficiency is roughly constant at a value of about $\nu = 0.2$. The threshold is most likely due to the sudden onset of radiative cooling in systems of high gravitational potential and was determined by Salz et al. [2016] to be:

$$\nu \cong const. \text{ for } v = -log_{10}(-\Phi_G) \leq 12.0 \tag{46}$$

The planet with the highest gravitational potential in the comparison-grid, has a value of $v = 9.4$, which is well below this threshold. It therefore is valid to assume the heating efficiency to be a constant.

Finally limits for the restricted Jeans parameter (see Section 2.3.2 and Fossati et al. [2017]) as well as the planetary density are introduced. As described in Kubyshkina et al. [2018a] planets with average densities below $30.0\frac{kg}{m^3}$ or above $20000\frac{kg}{m^3}$ are unlikely to exist and therefore excluded from the grid. Also planets with a value of $\lambda_0 < 10.0$ are excluded because of the lower boundary condition described in Section 3.7. Planets with a value of $\lambda_0 > 80.0$ are also excluded in accordance with Kubyshkina et al. [2018a] as they are assumed to have stable atmospheres. Using all this limits the comparison-grid contains 125208 theoretical planetary systems.

6 Analysis of the energy-limited approach

This chapter focuses on comparing different methods of obtaining atmospheric mass-loss rates with the energy-limited approach as well as how the resulting mass-loss rates depend on planetary parameters.

6.1 Comparison of different energy-limited mass-loss rates

In Section 2.4 three different ways of obtaining a particle escape rate with an energy-limited approach were introduced. The first two use the solutions of the energy-limited equations 20 and 21, while the third one simplifies the approach even further, by assuming the radius of XUV absorption to be equal to the planetary radius. Converting the escape rates to mass-loss rates, accounting for the Roche lobe effect by including the correction factor K and using the heating efficiency ν as well as the averaging factor $\frac{1}{4}$ on the total stellar XUV flux Φ_{XUV}, the three mass-loss rates can be computed with:

$$\dot{M}_{\zeta} = 4\pi \frac{\zeta \kappa_0 GMKm^2}{k^2 T_{eq}} \tag{47}$$

$$\dot{M}_{\lambda_1} = \pi \frac{\nu \Phi_{XUV} GMKm^2 R_{pl}}{k^2 T_{eq} \lambda_1^2} \tag{48}$$

$$\dot{M}_{R_{pl}} = \pi \frac{\nu \Phi_{XUV} R_{pl}^3}{GMK} \tag{49}$$

Figure 9 shows the ratio of $\dot{M}_{\zeta}$ and $\dot{M}_{\lambda_1}$ for all planets in the comparison-grid. The two methods result in very similar mass-loss rates for all systems. The maximum deviation can be observed for low values of the mass-loss rate with a maximum ratio of 1.14. With increasing mass-loss rates the deviations get smaller and the results are within 2% of each other for planets with high values of $\dot{M}$. These results indicate that in order to gain an order of magnitude estimate of $\dot{M}$, $\dot{M}_{\zeta}$ and $\dot{M}_{\lambda_1}$ are equally good estimators as the deviations between the two methods are well below one order of magnitude for all planets in the comparison-grid.

Figure 10 compares $\dot{M}_{\zeta}$ with $\dot{M}_{R_{pl}}$ and therefore visualizes the effects of the simplified energy-limited approach $r_1 = R_{pl}$. Again the deviations are the highest for planets with low $\dot{M}$ reaching up to an order of magnitude for planets with very low mass-loss rates. For planets with high mass-loss rates however, the two results are equal. This indicates that the $r_1 = R_{pl}$ simplification may be justified to be used as an order of magnitude estimation of $\dot{M}_{\zeta}$, although especially for very low values of $\dot{M}_{\zeta}$ an

underestimation must be expected. For calculated values of $\dot{M}_{R_{pl}}$ of less than $10^6 \frac{kg}{s}$ a correction by a factor of 2 or more should be used to estimate $\dot{M}_{\zeta}$.

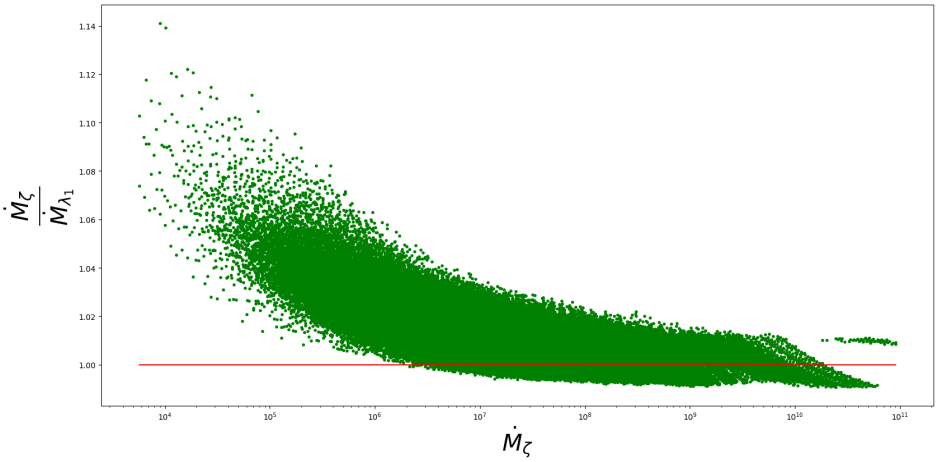

Figure 9: Ratio of mass-loss rates $\dot{M}_{\zeta}$ and $\dot{M}_{\lambda_1}$ obtained with energy-limited approaches. The red lines marks a ratio of 1.0

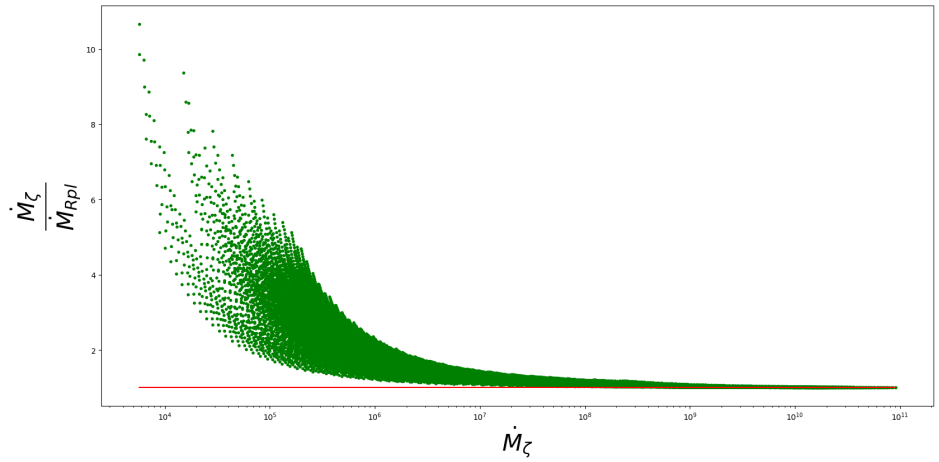

Figure 10: Ratio of mass-loss rates $\dot{M}_{\zeta}$ and $\dot{M}_{R_{pl}}$ obtained with energy-limited approaches. The red lines marks a ratio of 1.0

6.2 Estimated height of XUV absorption

Figure 11 compares the XUV absorption radius r_1 obtained with the energy-limited approach with the planetary radius R_{pl}. For high values of $\dot{M}$ the energy-limited approach estimates the XUV absorption to be at the planetary surface, while for low values it is estimated to be at up to 3 planetary radii. This does raise doubts on the applicability of the energy-limited approach especially on planets with high particle escape rates. While it does make sense that for more strongly heated planets (higher values of Φ_{XUV}) the absorption radius moves closer to the planet as a higher number density is needed to absorb all the incident stellar radiation, this would also imply very steep temperature profiles. The energy-limited approach assumes the temperature profile to have a $T = 0K$ minimum somewhere between the planetary radius and the XUV absorption layer (see Figure 7). A strongly heated absorption layer however would also result in higher temperatures at the absorption height, meaning the temperature in the atmosphere would first need to drastically cool by adiabatic cooling and then be reheated to even higher temperature values within a few hundred kilometers in the thermosphere.

Figure 12 shows that the XUV absorption radius is estimated especially close for systems with high incident stellar XUV flux. This means that the increase of the mass-loss rate with increasing Φ_{XUV} is slowed down by a decreasing XUV absorption height, which in turn means a smaller absorption cross-section πr_1^2.

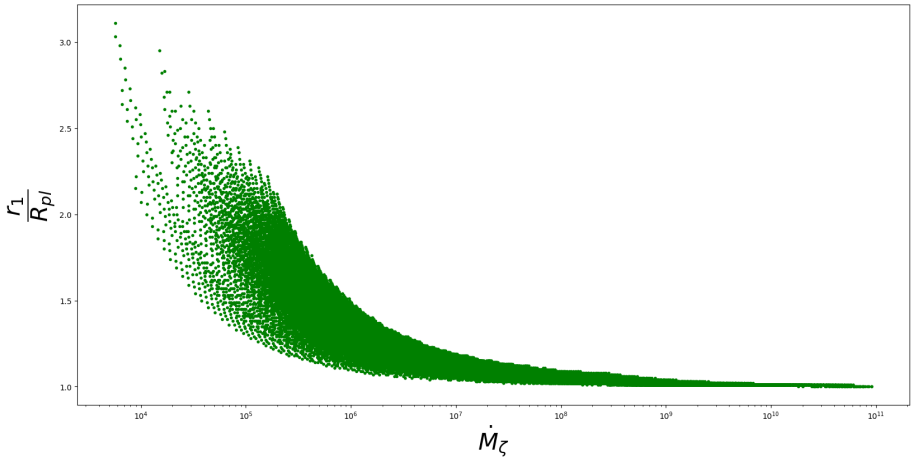

Figure 11: Ratio of XUV absorption radius r_1 obtained with the energy-limited approach and planetary radius R_{pl} for all planets in the comparison-grid.

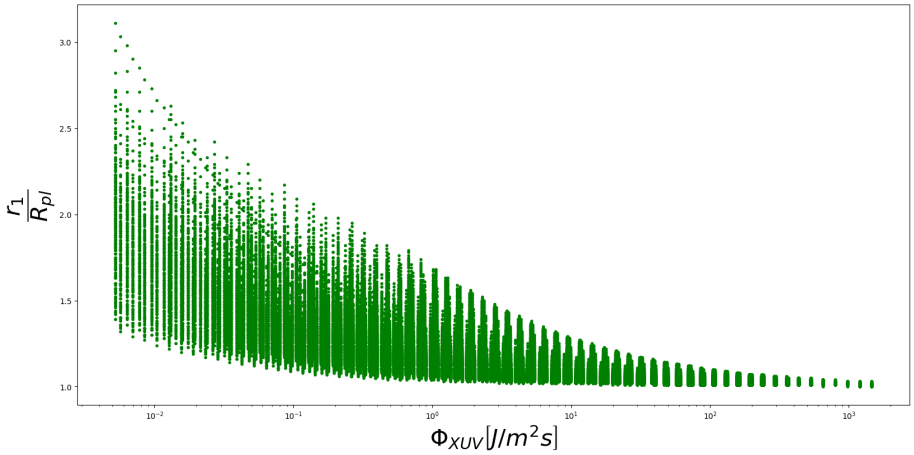

Figure 12: Ratio of XUV absorption radius r_1 obtained with the energy-limited approach and planetary radius R_{pl} over incident stellar XUV flux Φ_{XUV} for all planets in the comparison-grid.

The energy-limited formalism estimates smaller XUV absorption heights for increasing stellar XUV fluxes. In case of small irradiation by the star an absorption in higher regions is predicted, however the overall amount of energy input is small leading to moderate escape rates. In the case of strong irradiation on the other hand the energy is absorbed in the dense region near the planetary surface. The energy is therefore distributed to many individual particles and conduction is more efficient making steep temperature profiles as predicted in Figure 7 increasingly unlikely and limiting the temperature in the thermosphere. Figure 11 predicts that for strong irradiation especially high escape rates may be expected. However the approach also predicts especially close in absorption regions under these circumstances, which in turn make a steep temperature profile unlikely as the energy can be more easily distributed to the lower boundary.

6.3 Thermospheric temperatures

For hydrodynamic escape to happen, the absorbed XUV energy must only be distributed to so many particles that the energy gained per particle is high enough to overcome the gravitational potential of the planet. As introduced in chapter 2 and illustrated in Figure 7 the energy-limited approach assumes for the absorption layer to be high enough so that the particle density n within this region is small enough for this to happen. The higher the absorption layer, the smaller the particle density

and with that the more insufficient is conduction and the more energy is used per particle in the absorption layer to heat it to temperatures allowing for hydrodynamic escape. As stated in chapter 2 hydrodynamic escape is a continuous process in which the absorption of stellar energy is not used to accelerate one single particle but is used to heat the whole gas trough collisions until it reaches thermal energies larger than its potential energy and starts flowing upwards in a bulk.

To check the validity of the calculations Figure 13 compares the gravitational potential of a particle at r_1 with its thermal energy inferred by the temperature T_1 at r_1 estimated by the temperature profile equation 40. As in all of the considerations in Watson et al. [1981] the kinetic energy of the gas at r_1 is assumed to be negligible compared to its thermal energy. For planets with low gravitational potential and high irradiation the thermal energy at r_1 actually exceeds the gravitational potential. For the remaining systems the ratio is close to 1. This validates the calculations as the assumed temperatures reached at the XUV absorption height would indeed be high enough to overcome the gravitational energy of the planet.

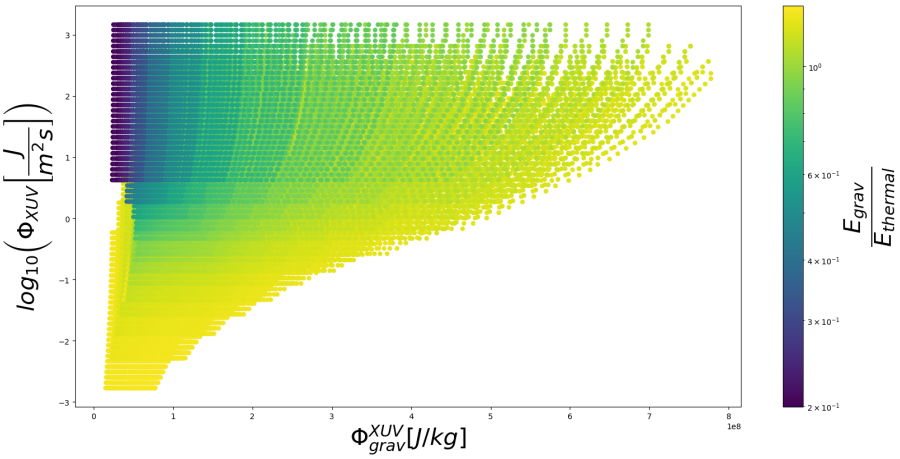

Figure 13: Visualization of the ratio of gravitational potential energy at the XUV absorption height to thermal energy at the absorption layer depending on the gravitational potential of the planet and the incident XUV flux.

For context Figure 14 shows the temperatures T_1 reached at r_1 in order to allow for hydrodynamic escape to happen. The temperature values at the XUV absorption height are of the order of 10^3 to 10^4 K and reach maximum values up to 50.000 K. This disfavours the energy-limited approach. For once the temperatures are especially high in highly irradiated systems with high gravitational potential. As mentioned above

these systems have especially low absorption heights close to the planetary surface. This would imply a temperature drop from the lower boundary to 0 K and then a sudden increase up to 50.000 K over a mere few hundred kilometers above the surface. In addition hydrodynamic simulations like Tian et al. [2005] and Murray-Clay et al. [2009] have found temperatures to remain significantly lower. The thermospheric temperatures of planets with low equilibirum temperatures remain below 1.000 K and those of Hot Jupiter type planets don't exceed 20.000 K. This indicates that the energy-limited approach most likely overestimates the thermospheric temperatures especially in highly irradiated systems with high gravitational potential, which in turn would imply an overestimation of the corresponding mass-loss rate.

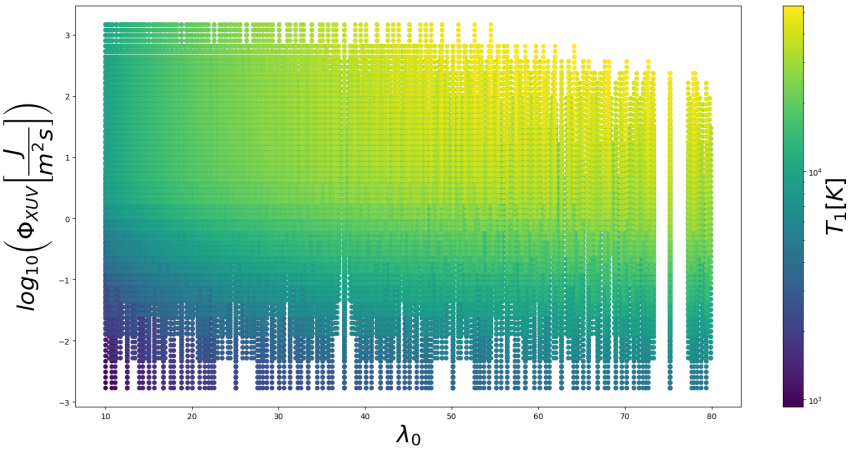

Figure 14: Visualization of the temperature at the XUV absorption layer depending on the lower boundary parameter λ_0 of the planet and the incident XUV flux

6.4 Absorption at unit optical depth

The energy-limited approach also completely lacks information on the actual absorption behaviour of the atmosphere. Besides not considering absorption profiles the energy-limited approach by Watson et al. [1981] does not at all consider the optical depth to XUV of hydrogen. To further validate the calculations the condition of unit optical depth to XUV should be compared with the resulting absorption heights and temperatures. In a static and isothermal atmosphere the condition of the level of unit optical depth to XUV would be [Watson et al., 1981]:

$$n_1 H_1 \sigma_{XUV} \approx 1 \tag{50}$$

$$H_1 = \frac{kT_1 r_1^2}{GMm} \tag{51}$$

Where n_1 is the particle density, H_1 the scale height and $\sigma_{XUV} \approx 5 \cdot 10^{-22} m^2$ [Erkaev et al., 2013] the absorption cross-section of atomic hydrogen to XUV. Because the atmosphere is not static but accelerating upwards and because the temperature is declining from r_1 upwards the true scale height is less than the value defined in equation 51 and the true condition would be [Watson et al., 1981]:

$$n_1 H_1 \sigma_{XUV} > 1 \tag{52}$$

Equation 50 can be used anyway to find an estimate of the pressure at the estimated XUV absorption height. Figure 15 illustrates the resulting pressure values. The overall structure does seem physical as the energy-limited approach estimates higher pressures for higher irradiation, which corresponds to an absorption deeper in the atmosphere. The optical depth to XUV in hydrogen atmospheres is 1 at about 10^{-9} bar (Murray-Clay et al. [2009]). As can be seen such pressures are only reached in the top right part of the plot. These are highly irradiated systems with high gravitational potential, but also with very low absorption regions, which as mentioned above imply overestimated thermospheric temperatures. In the remaining planetary systems the estimated pressures at r_1 are significantly lower.

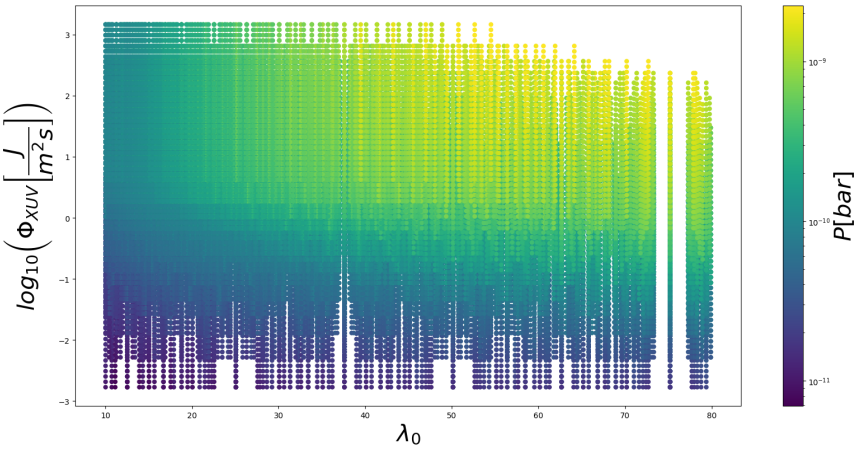

Figure 15: Estimated pressure at the XUV absorption layer depending on the gravitational potential of the planet and the incident XUV flux

6.5 Summary

To summarize the two methods of calculating energy-limited mass-loss rates by solving the energy-limited equations (escape based $\dot{M}_\zeta$ and absorption height based $\dot{M}_{\lambda_1}$) are equally good estimators as their deviations from another are well within an order of magnitude. Simplifying the energy-limited approach by choosing $r_1 = R_{pl}$ does seem to be justified within an order of magnitude, although an underestimation, especially in case of small mass-loss rates, should be expected. Figure 13 validates that the thermal energy reached at the absorption height is sufficient to overcome the gravitational potential of the planet. However, the estimated temperatures and pressures at the absorption layer do raise doubts on the applicability of the approach. The temperature profiles especially of highly irradiated planets would need to be very steep and especially for planets with high gravitational potential unphysical high temperatures would be needed. On the other hand for low irradiated planets the XUV absorption height might be estimated significantly different than the condition of unit optical depth to XUV would imply. All these consideration support the necessity of a more detailed comparison of the energy-limited results with hydrodynamic simulations.

7 Comparison of the energy-limited approach with hydrodynamic simulations

In 2018 Kubyshkina et al. [2018a] published a paper on a grid of upper atmosphere models. By using a one-dimensional hydrodynamic model, they were able to compute a grid of 7000 upper atmosphere models of hydrogen dominated atmospheres. From this grid they generated an interpolation routine that allows for the calculation of a variety of atmospheric parameters, including the mass-loss rate and the effective radius of XUV absorption, for planets within the grid limits. Their model does not only account for XUV driven hydrodynamic escape but for a variety of escape processes including Jeans escape and photochemical reactions within the upper atmosphere. This allows for the calculation of atmospheric mass-loss rates in all non-magnetic systems within the grid limits, no matter what escape process is dominant.

To investigate the validity of the energy-limited approach the mass-loss rates from this interpolation routine can be compared with the results of the energy-limited escape formalism. The aim is to find a limiting set of planetary parameters, within which the results of the Watson et al. [1981] algorithm comply with the results of the hydrodynamic model. Within this parameter range the energy-limited approach would be able to be considered a good approximation to the real mass-loss rate. Such a comparison is performed in this chapter. Since it was established in the previous chapter 6 that the different methods of obtaining energy-limited mass-loss rates all yield results within an order of magnitude of each other, $\dot{M}_\zeta$ will be used in this comparison to represent results obtained with the energy-limited approach. The mass-loss rates obtained by the Kubyshkina et al. [2018a] hydrodynamic simulations are denoted as $\dot{M}_{hc}$.

7.1 Dependence on mass-loss rates

Figures 16 and 17 illustrate that the ratio of the two escape rates is mainly determined by the simulation results $\dot{M}_{hc}$. The observed ratio range spawns from 10^{-5} to 10^{3}. As Figure 16 points out there is no obvious relation between the calculated ratio and $\dot{M}_\zeta$, which already indicates that it is impossible to estimate the ratio of mass-loss rates by only knowing $\dot{M}_\zeta$. Kubyshkina et al. [2018a] and Kubyshkina et al. [2018b] have also shown that $\dot{M}_{hc}$ can not be estimated with a simple function but has a rather complex behaviour depending on the combination of planetary parameters as different combinations yield different dominating processes. It is therefore not possible to derive a general law that is able to estimate the observed ratio $\frac{\dot{M}_\zeta}{\dot{M}_{hc}}$. Therefore this investigation will focus on describing the behaviour of the ratio within certain regimes of combinations of planetary parameters.

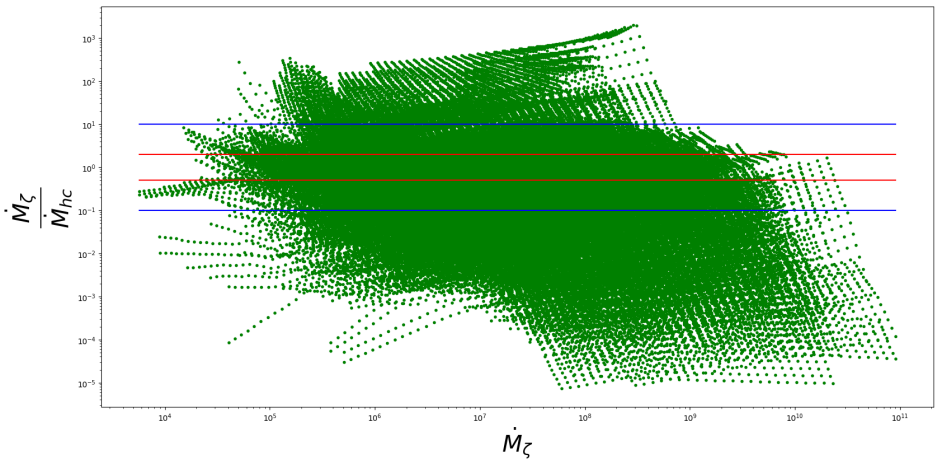

Figure 16: Ratio of mass-loss rates obtained with an energy-limited approach $\dot{M}_\zeta$ and hydrodynamic simulations $\dot{M}_{hc}$ compared to $\dot{M}_\zeta$. The red lines mark the area where the mass-loss rates are within a factor of 2 of each other. The blue lines mark the area where the mass-loss rates are within a factor of 10 of each other.

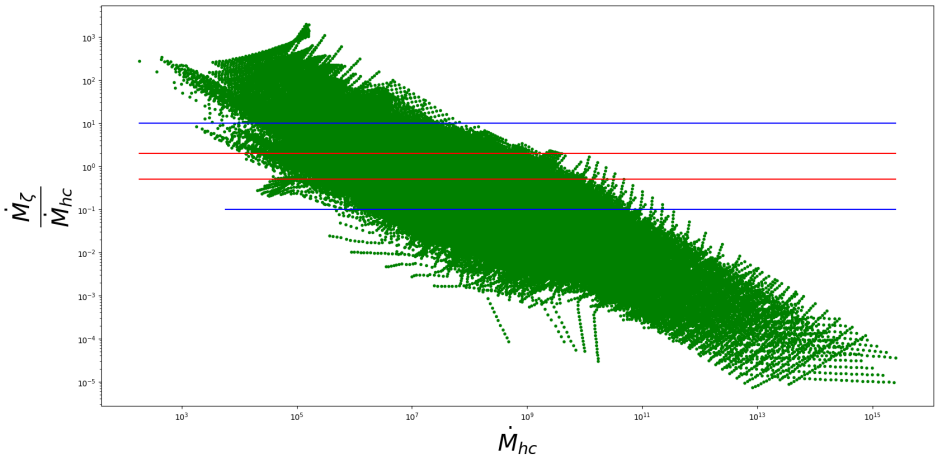

Figure 17: Ratio of mass-loss rates obtained with an energy-limited approach $\dot{M}_\zeta$ and hydrodynamic simulations $\dot{M}_{hc}$ compared to $\dot{M}_{hc}$. The red lines mark the area where the mass-loss rates are within a factor of 2 of each other. The blue lines mark the area where the mass-loss rates are within a factor of 10 of each other.

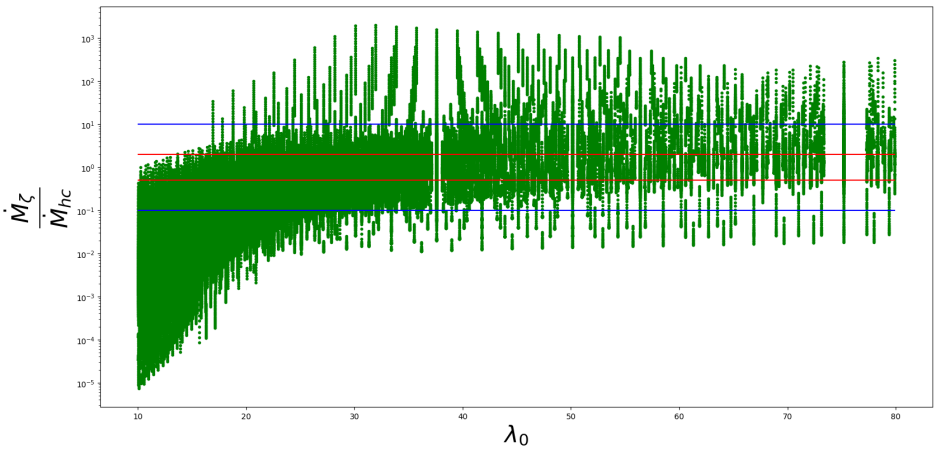

Figure 18: Ratio of mass-loss rates obtained with an energy-limited approach $\dot{M}_\zeta$ and hydrodynamic simulations $\dot{M}_{hc}$ compared to the lower boundary parameter λ_0. The red lines mark the area where the mass-loss rates are within a factor of 2 of each other. The blue lines mark the area where the mass-loss rates are within a factor of 10 of each other.

7.2 Dependence on λ_0 and T_0

The most important observation regarding the dependence of the ratio on planetary parameters can be obtained when comparing it with the lower boundary parameter λ_0, which in this case is chosen at the planetary surface with $r_0 = R_{pl}$ and $T_0 = T_{eq}$. Figure 18 displays the dependence of $\frac{\dot{M}_\zeta}{\dot{M}_{hc}}$ on λ_0. As can be observed for low values of λ_0, which correspond to low gravitational potentials of the planets, the energy-limited approach usually underestimates the correct mass-loss rate. In this regime drastic underestimation up to an order of 10^{-5} can be observed. This is probably due to the fact that in such systems the additional energy provided by XUV heating is sufficient to allow for *boil off* conditions in the lower parts of the atmosphere. Instead of adiabatically cooling the atmosphere near the lower boundary as expected by the energy-limited approach, all the absorbed XUV energy is used to heat the whole atmosphere from the bottom up. This way the thermal energy provided by the equilibrium temperature can be used in addition to the absorbed XUV energy to allow for energies high enough to escape close to the lower boundary. Since the absorbed energy is conducted downwards and is used to heat much denser regions, significantly higher escape rates can be observed. The energy-limited approach fails in this regime because it does not account for the fact that the gas already has almost reached

escape energies at the lower boundary. It completely disregards the already present thermal energy due to the equilibrium temperature of the planet and therefore tends to underestimate the mass-loss rate. This explanation is also supported by Figure 19. In the top left corner planets with very low gravitational potential and high temperatures are situated. This are the planets overestimated the most.

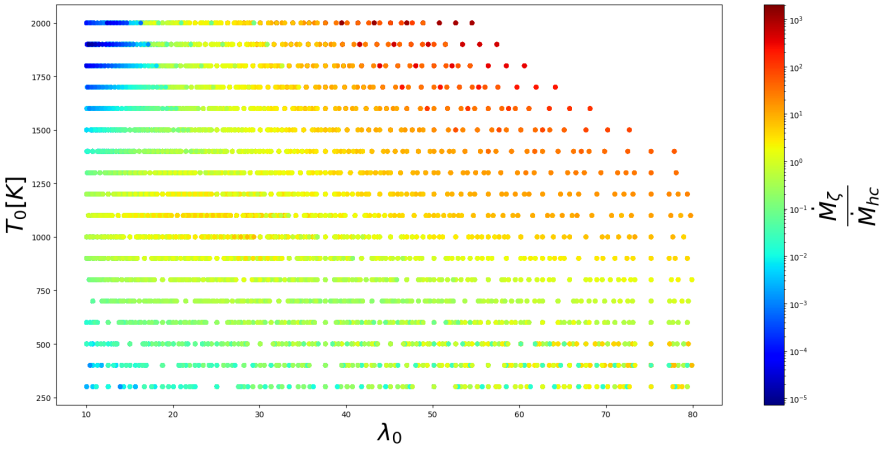

Figure 19: Ratio of mass-loss rates obtained with an energy-limited approach $\dot{M}_\zeta$ and hydrodynamic simulations $\dot{M}_{hc}$ compared to the lower boundary parameter λ_0 and the lower boundary temperature T_0.

With increasing values of λ_0 the planets leave the boil off regime and their mass-loss rates start to be dominated more by their gravitational potential. There is a transition region which roughly ends at a value of $\lambda_0 \approx 25$. From here on the behaviour of $\frac{\dot{M}_\zeta}{\dot{M}_{hc}}$ stays the same over the remaining range of λ_0. Both overestimation up to three orders of magnitude as well as underestimation up to 2 orders of magnitude can be observed. Overestimation is most prominent on planets with large gravitational potentials and high temperatures (see Figure 19). Figures 20 and 21 yield an explanation. The hydrodynamic simulations show that for large values of λ_0 the absolute magnitude of escape is mainly determined by the gravitational potential of the planet. For equal values of λ_0, planets with higher gravitational potential also have higher temperatures. The energy-limited approach does not account for this but actually estimates lower escape rates for equal values of λ_0 at hotter planets with lower gravitational potential. The simulated results on the contrary increase the mass-loss rate under the same circumstances as the gravitational potential is the driving factor. The magnitude of hydrodynamic escape is determined by the particle

density at the height were escaping energies are reached. For high mass planets this is mainly dominated by the gravitational potential as escape energies are only reached higher up in the atmosphere, where the number density is lower and therefore less particles are able to escape. The energy-limited approach tries to compensate this high gravitational potentials with very high thermospheric temperatures as seen in Figure 14. It basically asks how dilute does the gas need to be to be able to heat the absorption layer to escaping energies, while the simulations indicate that in fact escape energies are not reached at the absorption layer but only higher up where the gas is more dilute. The additional energy needed for escape is transported here by conduction.

Underestimation for high values of λ_0 can be explained similar. It can be mainly observed for low values of T_0. In this case for equal values of λ_0 the gravitational potential is lower which in turn allows for escape energies being reached in lower, more denser atmospheric heights. Again $\dot{M}_{hc}$ is mainly dominated by the gravitational potential in this regime which is not adequately accounted for by the energy-limited approach.

There are of course also a large sample of planets where the energy-limited approach does approximate the simulation results fairly reasonable. These can be found mainly in the intermediate regimes as the lower boundary parameter λ_0, which dominates the energy-limited mass-loss rate, here depicts the temperature-gravity relation the best and thermospheric temperatures are probably estimated quite well.

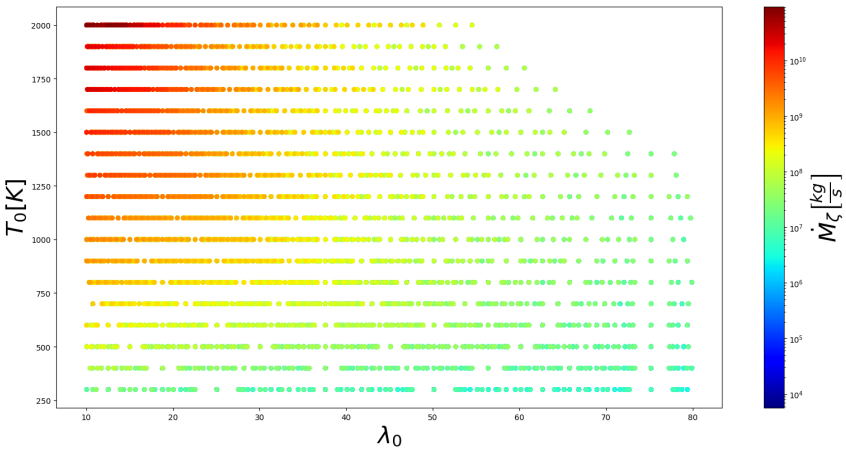

Figure 20: Visualization of the energy-limited mass-loss rate $\dot{M}_\zeta$ depending on the lower boundary parameter λ_0 and the lower boundary temperature T_0.

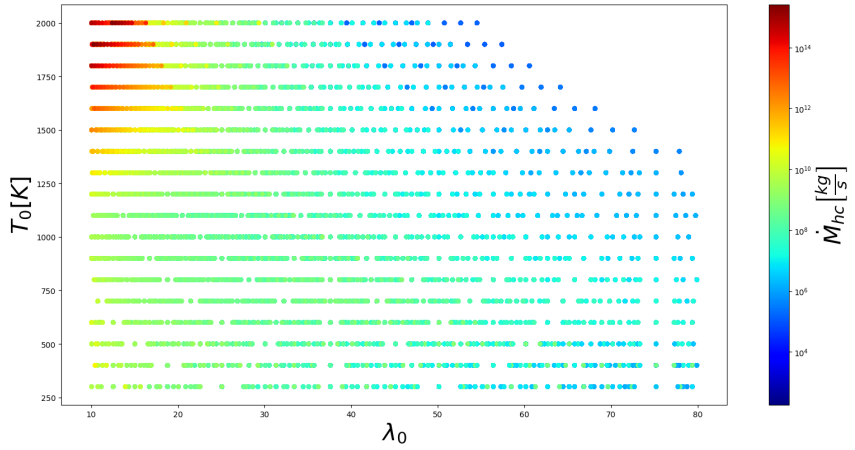

Figure 21: Visualization of the hydrodynamically simulated mass-loss rate $\dot{M}_{hc}$ depending on the lower boundary parameter λ_0 and the lower boundary temperature T_0.

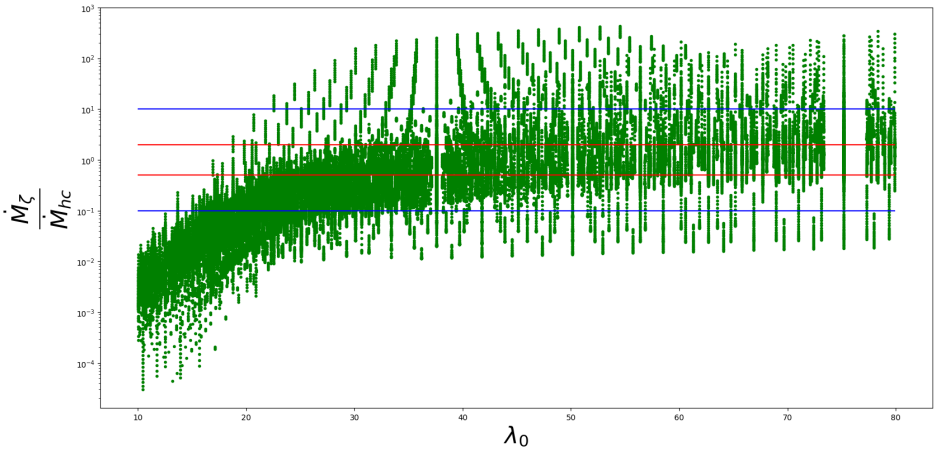

Figure 22: Ratio of mass-loss rates obtained with an energy-limited approach $\dot{M}_\zeta$ and hydrodynamic simulations $\dot{M}_{hc}$ compared to the lower boundary parameter λ_0. Only planets that comply with the subsonic condition are considered. The red lines mark the area where the mass-loss rates are within a factor of 2 of each other. The blue lines mark the area where the mass-loss rates are within a factor of 10 of each other.

Figure 22 is similar to Figure 18 but only depicts systems that comply with the subsonic condition equation 15. Complying with the condition does indeed remove planets, where the energy-limited approach performs the worst, from consideration. It mainly disregards strongly irradiated planets with low gravitational potential.

7.3 Dependence on Φ_{XUV}

Figure 23 highlights the behaviour of $\frac{\dot{M}_\zeta}{\dot{M}_{hc}}$ compared to the flux of stellar XUV radiation Φ_{XUV}. Again it can be observed that the ratio of mass-loss rates is mainly determined by the lower boundary parameter λ_0 and not by the magnitude of the stellar XUV flux. Figures 24 and 25 in comparison show the dependence of the individual mass-loss rates on both parameters. For values of $\lambda_0 > 40$ the simulated mass-loss rates $\dot{M}_{hc}$ do not depend any more on the magnitude of irradiation, but do seem to be only governed by the gravitational potential of the planet. Again the energy-limited approach does not account for that behaviour but estimates higher mass-loss rates for more strongly irradiated planets with equal values of λ_0. This results in overestimation for planets with high values of λ_0 and Φ_{XUV}. For values of $\lambda_0 < 20$ both mass-loss rates and therefore also their ratio is mainly determined by the stellar XUV flux. The highest observable escape rates can be found in highly irradiated systems with weak gravitational potentials. However, in the simulated case the mass-loss rates in these regime are up to 5 orders of magnitude higher than in the energy-limited case. This can be explained when considering that the temperature of the atmosphere most likely increases from the lower boundary upwards and does not first decrease and than increase steeply again. Especially in low gravity and high temperature systems a strong irradiation leads to energies sufficient for escape very close to the lower boundary, where the particle density is still very high. The energy-limited approach is not able to adequately estimate such boil off regimes reached because of the combination of low potential energy, high thermal energy and strong irradiation close to the lower boundary.

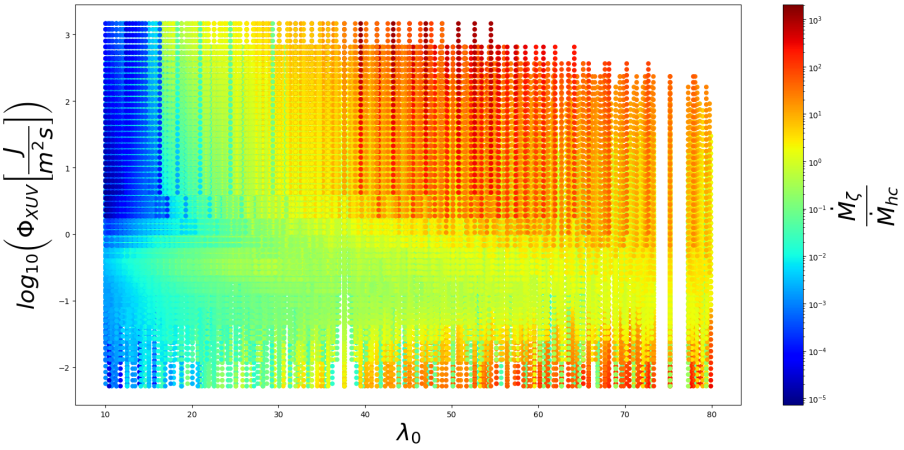

Figure 23: Ratio of mass-loss rates obtained with an energy-limited approach $\dot{M}_\zeta$ and hydrodynamic simulations $\dot{M}_{hc}$ depending on the lower boundary parameter λ_0 and the incident stellar XUV flux Φ.

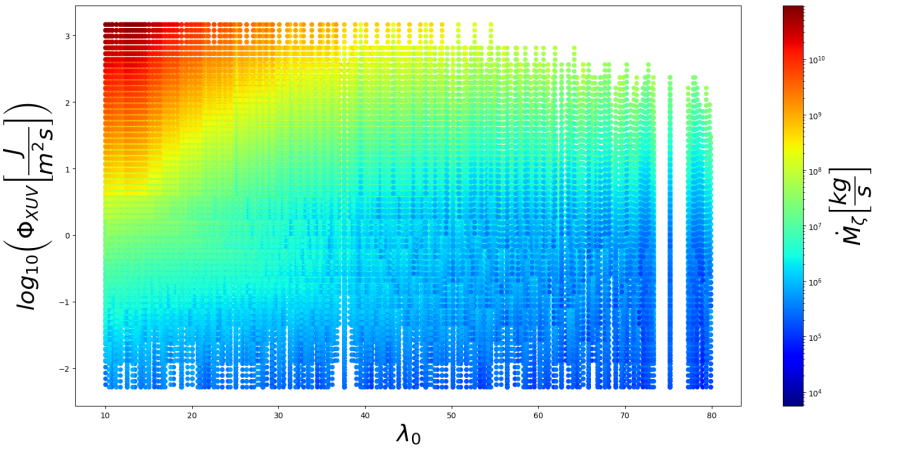

Figure 24: Visualization of the energy-limited mass-loss rate $\dot{M}_\zeta$ depending on the lower boundary parameter λ_0 and the incident stellar XUV flux Φ.

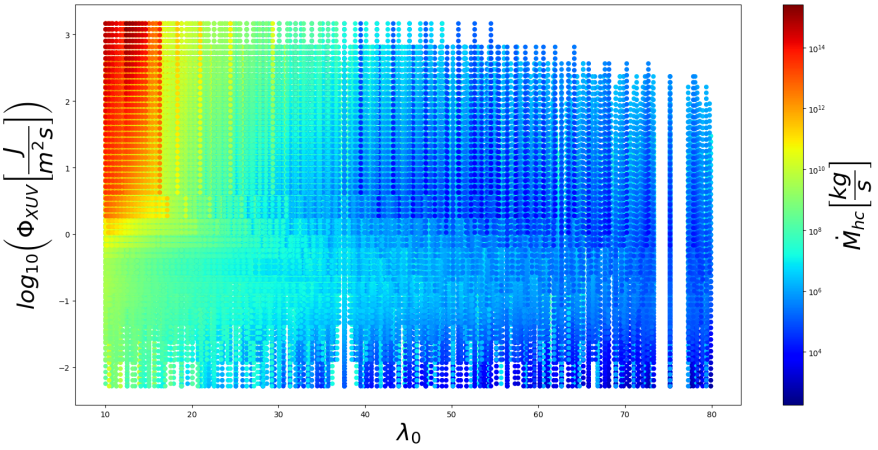

Figure 25: Visualization of the hydrodynamically simulated mass-loss rate $\dot{M}_{hc}$ depending on the lower boundary parameter λ_0 and the incident stellar XUV flux Φ.

7.4 Limiting conditions for certain overestimation

Using the gathered information two limiting conditions where certain overestimation as intended by Watson et al. [1981] is observed can be found. If either one of them is satisfied overestimation can always be expected for planets within the limits of the comparison-grid.

$$\lambda_0 \cdot \Phi_{XUV} \geq 42858 \frac{J}{m^2 s} \tag{53}$$

$$-\Phi_{grav} = \frac{GM_{pl}}{R_{pl}} \geq 6.26 \cdot 10^8 \frac{J}{kg} \tag{54}$$

7.5 Correctly estimated planets

Figure 26 gives an overview of all planets where $\dot{M}_{\zeta}$ and $\dot{M}_{hc}$ are within a factor of 2 of each other. This set contains about 30.000 planets or 24% of the comparison-grid. Figure 27 in comparison shows all planets where the two mass-loss rates are within a factor of 10 of each other. This set contains about 78.000 planets or 62% of the comparison-grid. It is important to remember the definition of the grid points when analyzing these plots. Per definition planets with a high equilibrium temperature are closer to their host star and therefore are also exposed to higher XUV fluxes. This

results in a natural cold to hot gradient with increasing Φ_{XUV}. Also planets which presumably have stable atmospheres have been eliminated from the grid, which in turn means the bottom right corner does not contain any grid points as these would be planets with very high gravitational potential but low equilibrium temperatures. Correctly estimated results can be found almost all over the parameter space except for planets with very low gravitational potential. As already mentioned previously, in this regime boil off conditions reached by a combination of thermal energy at the surface and additional XUV energy lead to drastic underestimation by the energy-limited approach.

Figure 28 shows all planets where the energy-limited estimation is off by more than one order of magnitude. Using all three plots intermediate equilibrium temperatures seem to result in fairly reliable estimations especially for planets with high gravitational potential. Figure 29 displays more closely the regime of all planets in the comparison-grid with equilibrium temperatures between 800 and 1300 K. Plotted are only planets where the energy-limited approach over- or underestimates the simulated mass-loss rates. Except for 6 planets, which most likely are an artefact of not exact simulation results, a gap in which the energy-limited approach always does estimate the simulated mass-lass rate up to an order of magnitude can be observed. For planets within the grid-limits and with equilibrium temperatures between 800 and 1300 K, Figure 29 can be used to check whether the system parameters of that specific planet are within this reliable estimation region.

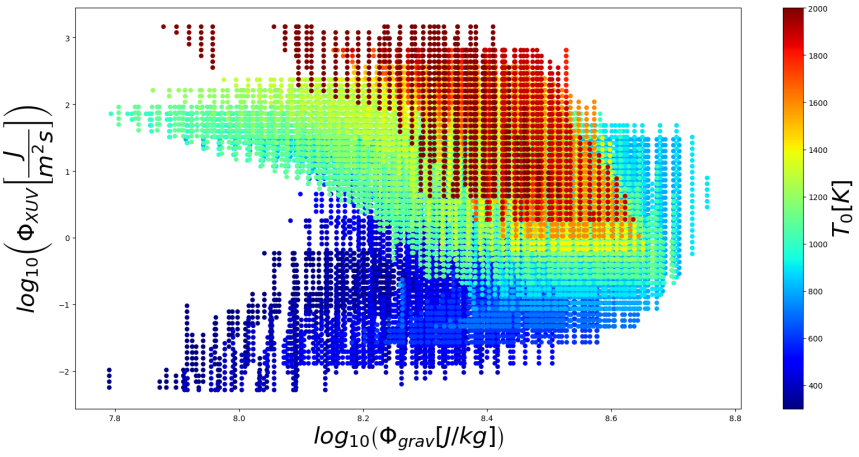

Figure 26: Overview of the system parameters of all planets where the energy-limited mass-loss rate and the mass-loss rate obtained by hydrodynamic simulations are within a factor of 2 of each other.

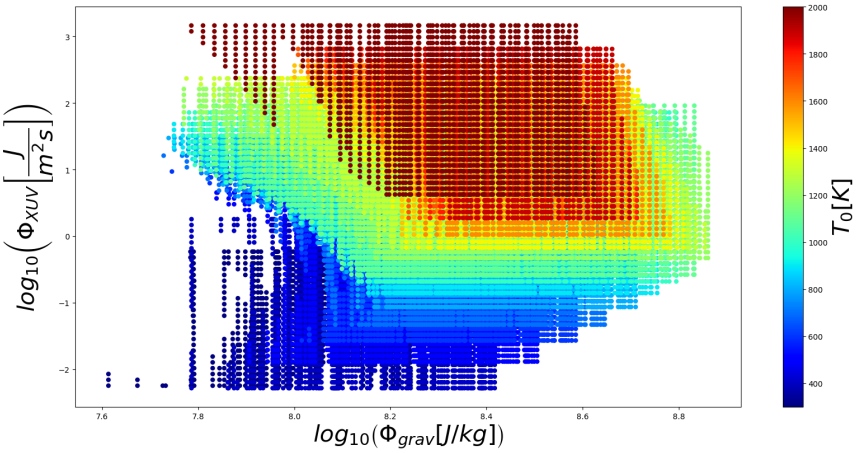

Figure 27: Overview of the system parameters of all planets where the energy-limited mass-loss rate and the mass-loss rate obtained by hydrodynamic simulations are within a factor of 10 of each other.

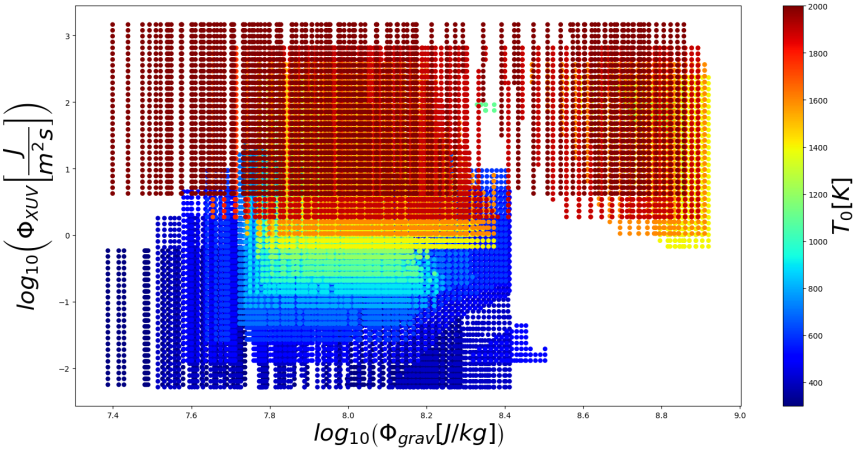

Figure 28: Overview of the system parameters of all planets where the energy-limited mass-loss rate and the mass-loss rate obtained by hydrodynamic simulations are different to each other by factor of 10 or more.

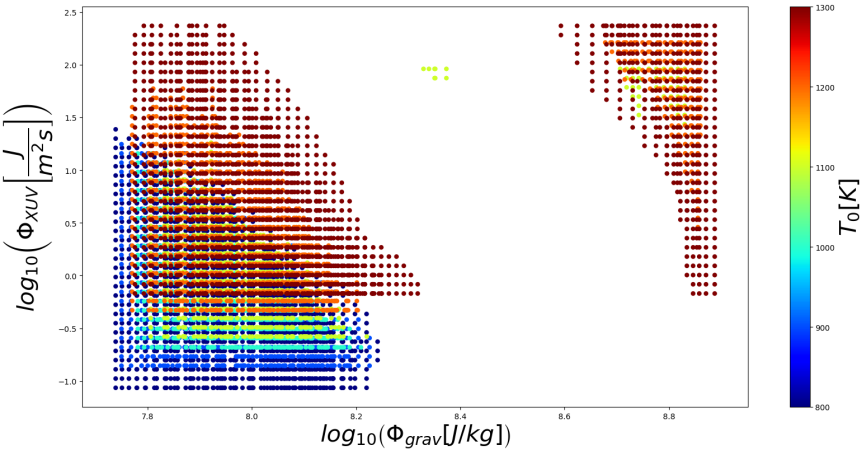

Figure 29: Overview of the system parameters of all planets with equilibrium temperatures between 800 and 1300 K and where the energy-limited mass-loss rate and the mass-loss rate obtained by hydrodynamic simulations are different to each other by factor of 10 or more.

7.6 Summary

To summarize this investigation has found significant differences between mass-loss rates obtained with the energy-limited approach and hydrodynamic simulations. The magnitude of $\dot{M}$ is mainly determined by the gravitational potential of the planet and is almost uneffected by large changes in the incident stellar XUV flux for values of $\lambda_0 > 40$. For planets with $\lambda_0 < 25$ boil off conditions can be reached close to the lower boundary as the absorbed additional energy is sufficient to heat the gas to escaping energies in low, dense atmospheric layers. The energy-limited approach is not able to account for both phenomena and is therefore unable to provide a reliable order of magnitude estimation of the true mass-loss rate $\dot{M}$. These results are in agreement with Kubyshkina et al. [2018b] results which also find strong underestimation for low values of λ_0 and both over- and underestimation for intermediate and high values of λ_0 (see Figure 30).

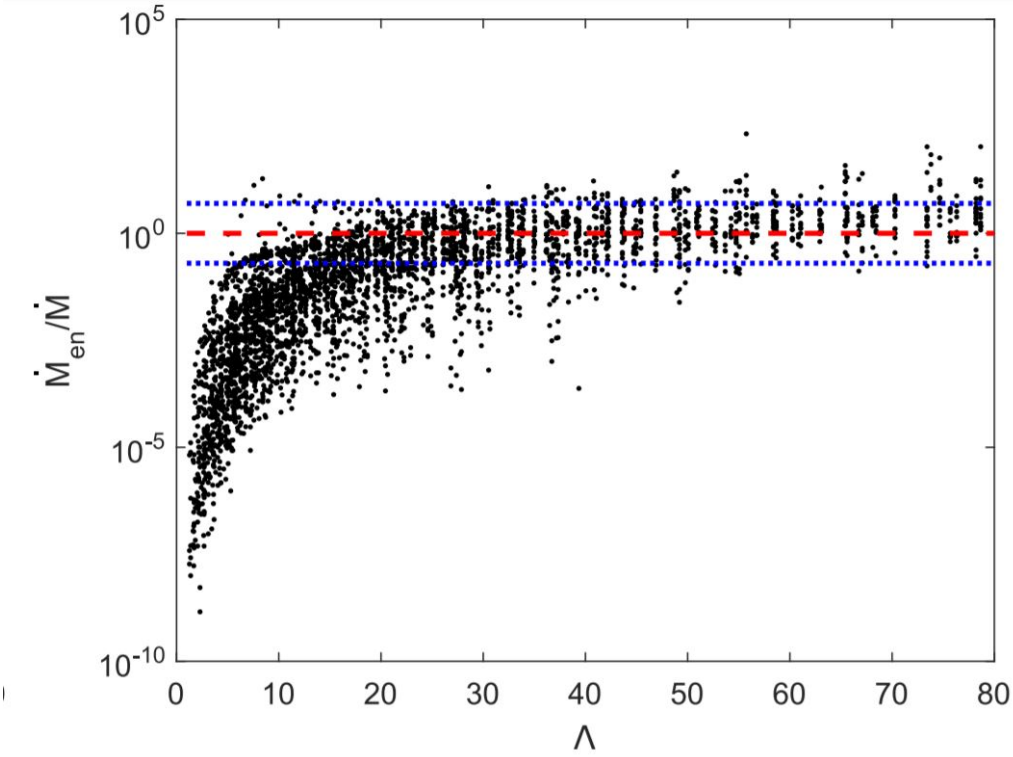

Figure 30: Comparison of an energy-limited mass-loss rate computed with XUV absorption radii obtained by hydrodynamic simulations and the simulated mass-loss rate $\dot{M}_{hc}$. The red line marks a ratio of 1, the blue lines the are where the two mass-loss rates are within a factor of 10 of each other. The figure was published in Kubyshkina et al. [2018b].

8 Conclusion

The investigation of the energy-limited atmospheric escape approach and its comparison with results of hydrodynamic simulations lead to the conclusion that the energy-limited escape approach in general is not a reliable order of magnitude estimator of the atmospheric mass-loss rate $\dot{M}$. However, for planets within the limits of the planetary grid defined in chapter 5 and with equilibrium temperatures of 800 to 1300 K, a reliable estimation of the mass-loss rate by the energy-limited approach can be expected, if the remaining planetary parameters of gravitational potential and incident XUV flux are within the region of the white gap in Figure 29. Above the following limits a certain overestimation of the mass-loss rate as indented by Watson et al. [1981] can be observed for all planets within the above mentioned planetary grid:

$$\lambda_0 \cdot \Phi_{XUV} \geq 42858 \frac{J}{m^2 s} \tag{55}$$

$$-\Phi_{grav} = \frac{GM_{pl}}{R_{pl}} \geq 6.26 \cdot 10^8 \frac{J}{kg} \tag{56}$$

Planets with $\lambda_0 > 40$ are mainly dominated by their gravitational potential, have low mass-loss rates and are mostly indifferent to the magnitude of incident stellar XUV radiation. For values of $\lambda_0 < 25$ the mass-loss rate is dominated by the incident stellar XUV flux leading to boil off conditions close to the planetary surface and high particle escape rates in strongly irradiated systems. In the intermediate regime of $25 < \lambda_0 < 40$ the two effects are of similar significance and the dominant process depends on the specific planetary parameters.

Besides the high number of assumptions and simplifications used in the derivation of the energy-limited formalism the main disadvantage of the approach is the assumed temperature profiles in the thermosphere. The energy-limited approach always assumes for the temperature to drop to a 0 K minimum before being reheated by XUV absorption. However, this can result in very steep temperature profiles and estimated absorption in regions not dense enough for the optical depth to XUV to have reached a value close to 1. More shallow temperature profiles and more moderate thermospheric temperatures in real atmospheres lead to an overestimation by the energy-limited approach. On the other hand if the planets thermal energy inferred from the equilibrium temperature is already close the energy needed for escape, the absorbed XUV energy can trigger boil off conditions near the lower boundary leading to very high particle escape rates and significant underestimation by the energy-limited approach.

References

Atreya, S. K., J. B. Pollack, and M. S. Matthews
1989. *Origin and evolution of planetary and satellite atmospheres.* University of Arizona Press.

Bauer, S. and H. Lammer
2004. *Planetary aeronomy: atmosphere environments in planetary systems.* Springer Science & Business Media.

Bodenheimer, P. and J. B. Pollack
1986. Calculations of the accretion and evolution of giant planets: The effects of solid cores. *Icarus*, 67(3):391–408.

Bollard, J., J. N. Connelly, M. J. Whitehouse, E. A. Pringle, L. Bonal, J. K. Jørgensen, Å. Nordlund, F. Moynier, and M. Bizzarro
2017. Early formation of planetary building blocks inferred from pb isotopic ages of chondrules. *Science advances*, 3(8):e1700407.

Borucki, W. J., D. Koch, G. Basri, N. Batalha, T. Brown, D. Caldwell, J. Caldwell, J. Christensen-Dalsgaard, W. D. Cochran, E. DeVore, et al.
2010. Kepler planet-detection mission: introduction and first results. *Science*, 327(5968):977–980.

Catling, D. C. and K. J. Zahnle
2009. The planetary air leak. *Scientific American*, 300(5):36–43.

Chamberlain, J. W.
1963. Planetary coronae and atmospheric evaporation. *Planetary and Space Science*, 11(8):901–960.

Coates, A.
2010. Atmospheric escape. `https://sci.esa.int/documents/33745/35957/1567258799920-Weihai-093-Coates-escape.pdf` Accessed: 19.12.2019.

Cubillos, P., N. V. Erkaev, I. Juvan, L. Fossati, C. P. Johnstone, H. Lammer, M. Lendl, P. Odert, and K. G. Kislyakova
2017. An overabundance of low-density neptune-like planets. *Monthly Notices of the Royal Astronomical Society*, 466(2):1868–1879.

Dermott, S. F.
1978. The origin of the solar system. *Origin of the Solar System.*

Erkaev, N., Y. N. Kulikov, H. Lammer, F. Selsis, D. Langmayr, G. Jaritz, and H. Biernat
2007. Roche lobe effects on the atmospheric loss from "hot jupiters". *Astronomy & Astrophysics*, 472(1):329–334.

Erkaev, N., H. Lammer, P. Odert, Y. N. Kulikov, and K. Kislyakova
2015. Extreme hydrodynamic atmospheric loss near the critical thermal escape regime. *Monthly Notices of the Royal Astronomical Society*, 448(2):1916–1921.

Erkaev, N. V., H. Lammer, P. Odert, Y. N. Kulikov, K. G. Kislyakova, M. L. Khodachenko, M. Güdel, A. Hanslmeier, and H. Biernat
2013. Xuv-exposed, non-hydrostatic hydrogen-rich upper atmospheres of terrestrial planets. part i: atmospheric expansion and thermal escape. *Astrobiology*, 13(11):1011–1029.

Fossati, L., N. Erkaev, H. Lammer, P. Cubillos, P. Odert, I. Juvan, K. Kislyakova, M. Lendl, D. Kubyshkina, and S. Bauer
2017. Aeronomical constraints to the minimum mass and maximum radius of hot low-mass planets. *Astronomy & Astrophysics*, 598:A90.

Gaudi, B. S.
2012. Microlensing surveys for exoplanets. *Annual Review of Astronomy and Astrophysics*, 50:411–453.

Izidoro, A., B. Bitsch, S. N. Raymond, A. Johansen, A. Morbidelli, M. Lambrechts, and S. A. Jacobson
2019. Formation of planetary systems by pebble accretion and migration: Hot super-earth systems from breaking compact resonant chains. *arXiv preprint arXiv:1902.08772*.

Jacobsen, S. B. and C. L. Harper
1996. Accretion and early differentiation history of the earth based on extinct radionuclides. *GEOPHYSICAL MONOGRAPH-AMERICAN GEOPHYSICAL UNION*, 95:47–74.

Jacobsen, S. B., M. C. Ranen, M. I. Petaev, J. L. Remo, R. J. O'Connell, and D. D. Sasselov
2008. Isotopes as clues to the origin and earliest differentiation history of the earth. *Philosophical Transactions of the Royal Society A: Mathematical, Physical and Engineering Sciences*, 366(1883):4129–4162.

Kitchin, C. R.
1987. *Stars, nebulae and the interstellar medium: observational physics and astrophysics*. CRC Press.

Kubyshkina, D., L. Fossati, N. Erkaev, C. Johnstone, P. Cubillos, K. Kislyakova, H. Lammer, M. Lendl, and P. Odert
2018a. Grid of upper atmosphere models for 1–40 m⊕ planets: application to corot-7 b and hd 219134 b, c. *Astronomy & Astrophysics*, 619:A151.

Kubyshkina, D., L. Fossati, N. V. Erkaev, P. E. Cubillos, C. P. Johnstone, K. G. Kislyakova, H. Lammer, M. Lendl, and P. Odert
2018b. Overcoming the limitations of the energy-limited approximation for planet atmospheric escape. *The Astrophysical Journal Letters*, 866(2):L18.

Lammer, H.
2013. *Origin and evolution of planetary atmospheres: Implications for habitability.* Springer Science & Business Media.

Lammer, H., N. Erkaev, L. Fossati, I. Juvan, P. Odert, P. Cubillos, E. Guenther, K. Kislyakova, C. Johnstone, T. Lüftinger, et al.
2016. Identifying the 'true'radius of the hot sub-neptune corot-24b by mass-loss modelling. *Monthly Notices of the Royal Astronomical Society: Letters*, 461(1):L62–L66.

Lammer, H., M. Leitzinger, M. Scherf, P. Odert, C. Burger, D. Kubyshkina, C. Johnstone, T. Maindl, C. Schäfer, M. Güdel, et al.
2020. Constraining the early evolution of venus and earth through atmospheric ar, ne isotope and bulk k/u ratios. In *Icar*, volume 339, P. 113551.

Lammer, H., A. Stökl, N. Erkaev, E. Dorfi, P. Odert, M. Güdel, Y. N. Kulikov, K. Kislyakova, and M. Leitzinger
2014. Origin and loss of nebula-captured hydrogen envelopes from 'sub'-to 'super-earths' in the habitable zone of sun-like stars. *Monthly Notices of the Royal Astronomical Society*, 439(4):3225–3238.

Lammer, H., A. L. Zerkle, S. Gebauer, N. Tosi, L. Noack, M. Scherf, E. Pilat-Lohinger, M. Güdel, J. L. Grenfell, M. Godolt, et al.
2018. Origin and evolution of the atmospheres of early venus, earth and mars. *The Astronomy and Astrophysics Review*, 26(1):2.

Luger, R. and R. Barnes
2015. Extreme water loss and abiotic o2 buildup on planets throughout the habitable zones of m dwarfs. *Astrobiology*, 15(2):119–143.

Mayor, M. and D. Queloz
1995. A jupiter-mass companion to a solar-type star. *Nature*, 378(6555):355–359.

Montmerle, T., J.-C. Augereau, M. Chaussidon, M. Gounelle, B. Marty, and A. Morbidelli
2006. 3. solar system formation and early evolution: the first 100 million years. *Earth, Moon, and Planets*, 98(1-4):39–95.

Moutou, C., M. Deleuil, T. Guillot, A. Baglin, P. Borde, F. Bouchy, J. Cabrera, S. Csizmadia, H. J. Deeg, et al.
2013. Corot: Harvest of the exoplanet program. *Icarus*, 226(2):1625–1634.

Murray-Clay, R. A., E. I. Chiang, and N. Murray
2009. Atmospheric escape from hot jupiters. *The Astrophysical Journal*, 693(1):23.

NASA, A. R. C.
2017. Exoplanet discoveries. `https://www.nasa.gov/image-feature/ames/exoplanet-discoveries` Accessed: 21.05.2020.

Owen, J. E. and Y. Wu
2013. Kepler planets: a tale of evaporation. *The Astrophysical Journal*, 775(2):105.

Owen, J. E. and Y. Wu
2016. Atmospheres of low-mass planets: the "boil-off". *The Astrophysical Journal*, 817(2):107.

O'Brien, D. P., K. J. Walsh, A. Morbidelli, S. N. Raymond, and A. M. Mandell
2014. Water delivery and giant impacts in the 'grand tack'scenario. *Icarus*, 239:74–84.

Parker, E.
1964. Dynamical properties of stellar coronas and stellar winds. i. integration of the momentum equation. *The Astrophysical Journal*, 139:72.

Pollack, J. B., O. Hubickyj, P. Bodenheimer, J. J. Lissauer, M. Podolak, and Y. Greenzweig
1996. Formation of the giant planets by concurrent accretion of solids and gas. *icarus*, 124(1):62–85.

Safronov, V. and E. Zvjagina
1969. Relative sizes of the largest bodies during the accumulation of planets. *Icarus*, 10(1):109–115.

Salz, M., P. Schneider, S. Czesla, and J. Schmitt
2016. Energy-limited escape revised-the transition from strong planetary winds to stable thermospheres. *Astronomy & Astrophysics*, 585:L2.

Shematovich, V. I., D. E. Ionov, and H. Lammer
2014. Heating efficiency in hydrogen-dominated upper atmospheres. *Astronomy & Astrophysics*, 571:A94.

Stökl, A., E. A. Dorfi, C. P. Johnstone, and H. Lammer
2016. Dynamical accretion of primordial atmospheres around planets with masses between 0.1 and 5 m$\oplus$ in the habitable zone. *The Astrophysical Journal*, 825(2):86.

Tian, F., O. B. Toon, A. A. Pavlov, and H. De Sterck
2005. Transonic hydrodynamic escape of hydrogen from extrasolar planetary atmospheres. *The Astrophysical Journal*, 621(2):1049.

Tu, L., C. P. Johnstone, M. Güdel, and H. Lammer
2015. The extreme ultraviolet and x-ray sun in time: High-energy evolutionary tracks of a solar-like star. *Astronomy & Astrophysics*, 577:L3.

Valencia, D., M. Ikoma, T. Guillot, and N. Nettelmann
2010. Composition and fate of short-period super-earths-the case of corot-7b. *Astronomy & Astrophysics*, 516:A20.

Volkov, A. N. and R. E. Johnson
2013. Thermal escape in the hydrodynamic regime: Reconsideration of parker's isentropic theory based on results of kinetic simulations. *The Astrophysical Journal*, 765(2):90.

Volkov, A. N., R. E. Johnson, O. J. Tucker, and J. T. Erwin
2011. Thermally driven atmospheric escape: Transition from hydrodynamic to jeans escape. *The Astrophysical Journal Letters*, 729(2):L24.

Walsh, K. J., A. Morbidelli, S. N. Raymond, D. P. O'Brien, and A. M. Mandell
2011. A low mass for mars from jupiter's early gas-driven migration. *Nature*, 475(7355):206.

Wang, H., B. P. Weiss, X.-N. Bai, B. G. Downey, J. Wang, J. Wang, C. Suavet, R. R. Fu, and M. E. Zucolotto
2017. Lifetime of the solar nebula constrained by meteorite paleomagnetism. *Science*, 355(6325):623–627.

Watson, A. J., T. M. Donahue, and J. C. Walker
1981. The dynamics of a rapidly escaping atmosphere: applications to the evolution of earth and venus. *Icarus*, 48(2):150–166.

Wetherill, G. W.
1980. Formation of the terrestrial planets. *Annual review of astronomy and astrophysics*, 18(1):77–113.

Yelle, R. V.
2004. Aeronomy of extra-solar giant planets at small orbital distances. *Icarus*, 170(1):167–179.